12-5-2018

Modeling and Extraction of Transport Parameters to Simulate Drug Delivery in the Murine Cochlea

Kevin Wilson
kw8745@rit.edu

RIT

Modeling and Extraction of Transport Parameters to Simulate Drug Delivery in the Murine Cochlea

by

Kevin Wilson

A thesis submitted in partial fulfillment of the
requirements for the degree of
Master of Science in Electrical Engineering

Department of Electrical Engineering
Kate Gleason College of Engineering
Rochester Institute of Technology
Rochester,NY
December 5th, 2018

Comittee Approval:

Dr. David A. Borkholder *Date*

Thesis Advisor

Dr. Nathan D. Cahill *Date*

Co-Advisor

Dr. Majid Rabbani *Date*

Committee Member

Dr. Sohail A. Dianat *Date*

Dept. Head, Electrical Engineering

Abstract

The usage of 1D and 3D models to simulate drug transport through the inner ear is a prominent method in cochlear fluid pharmacokinetics. However, the data used to create these models, is often based on invasive sampling methods that limit the spatial resolution given the size of the cochlear compartments within which solute can be measured. In this work by leveraging 3-D registered micro-Computed Tomography (μCT) scans of the murine cochlea that have been taken as iodinated contrast agent is delivered to it, we extract transport parameters and simulate a forward 1D model that allows variable and pulsatile delivery profiles over time and can be extended to the use of other drugs.

Our 1D model may be used to simulate transport of a compound within the primary scalae or compartments of the cochlea namely: scala tympani (ST), scala vestibuli (SV) and scala media (SM). We investigate extracting transport parameters of the 1D model for the iodinated contrast agent (Iopamidol), such as the concentration dependent diffusion coefficient, along with permeabilities across membranes that represent transfer between the primary scalae and clearance out to blood. Flow rates that change over time are also learned, to account for leakage due to experimental set up. Dimensions of cochlear structures considered in the model, and empirical concentration profiles are extracted non-invasively over regional cross sections of a set of registered μCT scans of the mouse cochlea while an Iodinated contrast agent (Iopamidol) is delivered to it. Given initial estimates of the transport parameters, we use a simple iterative gradient descent approach to minimize the mean-squared error between our predicted concentrations from the 1D model and those derived empirically. We put forth a method to illustrate that once these parameters are learned for the contrast agent, they can be adjusted to simulate the delivery of other compounds, and can also be used to study various infusion paradigms to maintain a suitable therapeutic window for optimal, effective and safe administration of a drug. The results are important in the development of such paradigms for the prevention and treatment of acute and chronic types of hearing loss.

Acknowledgements

I am extremely grateful to my advisor Dr. David A. Borkholder for his tutelage and support throughout this project.

I would like to thank Dr. Nathan D. Cahill who was almost like another advisor to me.

I wish to extend my gratitude to Dr. Majid Rabbani for taking the time to be on my committee and for being an amazing teacher during my time at RIT.

I wish to thank Sanketh Moudgalya at RIT, and the team at the University of South Florida, without whom this project would not be possible. I also acknowledge the support of the National Institute On Deafness and Other Communication Disorders of the National Institutes of Health through grant R01DC014568.

My heartfelt gratitude to my father and my late mother for all that they have done; and to my friends, family and wellwishers for their continued support throughout.

Contents

List of Figures

List of Tables

List of Symbols

Symbol	Description	Units
j	Molar flux	$mg/mm^2 s$
D	Diffusion coefficient	mm^2/s
c	Concentration	mg/ml
x	Direction of longitudinal transport	mm
y, z	Directions perpendicular to longitudinal transport	mm
$\bar{c}$	Average concentration across a cross section of a tube	mg/ml
c_0	Concentration at time instance 0	mg/ml
$\bar{b}$	Average concentration in cross section of neighboring tube	mg/ml
v	Velocity of solution in a tube	mm/s
t	time	s
k_B	Boltzmann's constant	J/K
T	Temperature	K
η	viscosity of solution into which solute is diffusing	P
r_H	Hydrodynamic radius	m
MW	Molecular weight of solute	gm/mol
$\mathcal{N}_0$	Avogadro's number	/mol
ρ	Density of solute	g/cc^3
$c_{v/v}$	concentration in volume/volume terms	-
D_0	limit of diffusion coefficient when concentration tends to 0	mm^2/s
γ	Drop-off parameter in concentration dependent diffusion coefficient	-
F	Volumetric Flow rate	nL/s
S	Cross sectional Area	mm^2
L	length of tube	m
ω	membrane permeability	mol/N s
R	gas constant	J/mol K
K	Permeation or transfer coefficient	mm/s
A	area of membrane between regions	mm^2

$\mathscr{L}$	Mean squared Error of normalized extracted and simulated concentrations	-
n	discretized notation in space for x	-
i	discretized notation for time	-
I	total number of discrete time steps	-
N	total number of discrete distance steps	-
$C(n)$	concentration temporally averaged over 20 min at point n	mg/ml
$C_{scan}(n)$	concentration extracted from 20 min μCT scan at point n	mg/ml
α_K	learning rate for transfer coefficients	mm^2/s^s
α_γ	learning rate for drop-off parameter	-
α_{D_0}	learning rate for D_0	mm^4/s^2
α_F	learning rate for volumetric flow rate	nL^2/s^2

1 Introduction

The mammalian inner ear consists of three main structures, the semicurcular canals, the vestibule and the cochlea. While the vestibule and the canals are important for vestibular functions, the cochlea is important for auditory fucntions. The cochlea is a coiled bony structure that handles transduction of mechanical sound waves to a neural response. It is comprised of various compartments: scala tympani (ST), scala vestibuli (SV) and scala media (SM). The mechanical stimulation of the membrane between ST and SM and the structures on it, result in the transduction of mechanical to electrical (neural) response. The hair cells on the membrane and the structures associated with it are important components in this transduction, and most drug based therapeutic interventions are aimed at delivery to these cells. Drug delivery can either be systemic (oral, intramuscular, intravenous) or, directed or local delivery, but site directed delivery is usually preferred since it avoids issues with overcoming the blood-labyrinth barrier and systemic side effects.

1.1 Current uses for inner ear drug delivery

Drug delivery to the inner ear has the potential to treat auditory and vestibular diseases [1]. The use of gentamicin for the treatment of Meniereâs, a vestibular disease is one of the more notable examples of drugs being delivered to the inner ear. Another one is the use of steroids for sudden sensorineural hearing loss, an auditory disease. These drugs are more commonly delivered to the middle ear so that they may be absorbed by the inner ear through the round and oval window membrane [2]. RNA Interference and Stem-cell therapy are promising technologies that are being developed but need direct delivery to the inner ear[3]. For the purpose of delivery, microsystem technologies for cochlear implants are an emerging development so that drugs may be applied more precisely and for longer durations and with controlled infusion profiles [1, 2]. Due to space constraints, and the difficulties associated with measuring drug levels in the inner ear, application protocols tend to be empirically based with large ranges of suggested doses as in the case of gentamicin [4]. This also leads to wide variations in reports of loss of hearing experienced by patients. These variations warrant the need for modelling pharmacokinetics in the inner ear to better understand the distribution of drugs within it.

1.2 Methods in sampling

Sampling refers not only to the sampling of fluid concentrations within the cochlea but also to the sampling of cochlear structure and compartment dimensions.

1.2.1 Sampling of drug concentration

A common method in the study of inner ear pharmacokinetics estimates the drug concentration based on functional assessment of hearing [5]. It relies on the assumption that the concentration is proportional to the physiological response of the drug and that the sensitivity of cochlear hair cells is uniform throughout the inner ear. The basilar membrane responds to different frequencies in the range of hearing along its length. Audiograms are plotted at different points in time along the course of drug delivery, and observations are made based on shifts in hearing related to concentration. A tonotopic map is used to correlate the location in space along the basilar membrane to the frequency shift observed. For the evaluation of various infusion protocols, the indirect methods provide useful qualitative information but only provide estimates of concentration profiles.

Another approach involves markers being applied to the fluid spaces and their spread documented using ion selective electrodes or fluid samples taken from the basal or apical turns of the cochlea [6, 7, 8]. These methods are invasive and may interfere with the concentration values. While the spatial density depends on number of electrodes used, the size of the structures being studied limits the number to 2 or 3. Their applicability further reduces in smaller animals.

Haghpanahi et al. sampled concentrations at 5 points along the length of SV and ST using a set of 2D uCT images [9]. Since they had low resolution, they were registered to Santi et al's labelled atlas scans [10]. This method is non-invasive and can be extended to provide higher spatial resolution.

1.2.2 Sampling of cochlear dimensions

Methods for extractions of cochlear dimensions so far have been based on Magnetic resonance microscopy (MRM) scans of chochleae of multiple species that were treated and fixed with various agents over a few days [11, 12]. Once treated the MRM scans were taken of the excised temporal bones and the different regions of the cochleae were segmented from each slice using density thresholds and investigator intervention. Planes were interpolated by rotating them about the central axis of the helical cochlear structure and extracting the areas about the midpoint of each intersection of a scala with the plane. This method

is invasive and does not ensure that the area extracted at each point along the length is the true cross sectional area of the scala since it uses the helical axis (or the rotational axis) as reference. A true cross sectional plane would be perpendicular to the medial axis of the cochlea (in this case the helix that describes the cochlea) at the point of interest.

1.3 Forward models

A good forward model would be able to provide us with close estimates of how the drug propagates, which could allow us to tweak our rate of injection so that it results in a suitable balance between efficacy and toxicity for each individual case. This would be particularly useful in the use of implantable pumps where the delivery profile can be controlled.

The Washington University cochlear fluid simulator, also known as FluidSim [13], is a detailed 1D model has been developed to simulate cochlear pharmacokinetics in a variety of small mammals and humans with various drug delivery configurations . It divides each scala into 0.1mm sections along the length and takes into account diffusion, interscala communications, longitudinal flow and clearance. Delivery is allowed by various methods such as permeation through the round window, injection into the perilymph at low rates and perfusion via a cochleostomy. A leakage with a fixed flow rate over the course of delivery can also be considered. While the simulator is well detailed, it does have some limitations. The diffusion coefficient is fixed and does not have the provision to be allowed to change with the concentration of the solute which is important for transport of substances at higher concentrations. It is also based only on molecular weight and does not take into account density of the solute; this implies that different solutes with the same molecular weight would have similar transport characteristics which may not be the case. It makes use of average half-times that can be normalized by area to denote interscala communication, while clearance half-times are assumed to be constant along the length of the scalae. The model provides some demos for certain drugs, with preset transfer and clearance paramaters. But to simulate transport for a new drug, these half times need to be estimated and set by the user and experiments need to be performed to derive clearance half-times.

Plontke et. al simulated a finite element simplified 3D model based on the guinea pig cochlea and demonstrated the existence of substantial radial gradients across the basal turn especially for larger animals [14]. These gradients are insignificant in cochlear regions of smaller cross sections or even those of smaller animals. The model consisted of multiple straight tapered tubes connected to each other to represent the guinea pig cochlea. The 3D structure of the model was simple. By reducing the dimension-

ality of the geometry, it was possible to simulate a 1D model and to compare it to FluidSim. The model works well to show the radial concentration gradients within the basal region of each scala. The parameters used in the model are based on earlier derived transfer coefficients from FluidSim. They suggest that methods to validate the radial gradients within the basal regions are few and include using ion selective microelectrodes. The model is also suggested to be innacurate due to the simplification of the 3D structure. With the computational complexity involved, estimation of parameters becomes cumbersome since the simulation needs to be run multiple times which leads them to suggest that reduced 1D models will be the preferred method for use in pharmacokinetics for now. This model too does not take into account the possibility of a concentration dependent coefficient of diffusion and is limited to demonstrating the use of bolus or continuous delivery of drug.

1.4 Our work

Through this work we design a 1D model based on the mouse cochlea, which depends on transport parameters such as a concentration dependent diffusion coefficient, transfer coefficients between scalae and clearance out to blood. To extract these parameters we make use of 3D registered μCT scans of the mouse cochlea taken over time as it is infused with an iodinated contrast agent (Iopamidol) through a cochleostomy. The registration of these scans with high spatial resolution aids in identifying membranes and individual scalae, and provides an accurate and non-invasive method of sampling (both the concentrations as well as the cochlear dimensions) using the medial axes of the scalae. This does not disrupt the natural state of transport within the cochlea. We randomly initialize the estimates of the transport parameters and optimize them with a simple gradient descent approach. The method minimizes the mean square error between our simulations and concentration profiles extracted from 3D registered μCT scans by adjusting the parameter estimates at a rate proportional to the rate of change of the error with respect to that parameter. Leakage within each experiment is also estimated by this method. We extend the use of the model by adjusting the extracted parameters to simulate profiles for other drugs and also illustrate its use in optimizing delivery profiles for a target notational therapeutic window.

1.5 Overview

Chapter 2 starts by providing an overview of the structure of the mammalian ear and then goes on to explain the structure and functioning of the inner ear in some detail. This is followed by an explanation of

the pharmacokinetics of the inner ear in chapter 3 and lays out the partial differential equations (PDEs) used. Chapter 4 describes the process involved in the extraction of data in our experiments, beginning with an outline of the surgical procedures for the delivery of contrast agent and the imaging performed on the mouse. It then explains the process of registration followed by the concentration extraction. Chapter 5 discusses the optimization technique by first addressing the discretization of the the earlier discussed PDEs followed by the gradient descent method. Chapter 6 for the results, talks about the extracted concentrations and parameters learned from them. The parameters are then used to illustrate applications of the model. We conclude with the final chapter and discuss future work within our lab.

The flowchart below provides an outline of the process that will be detailed in the thesis.

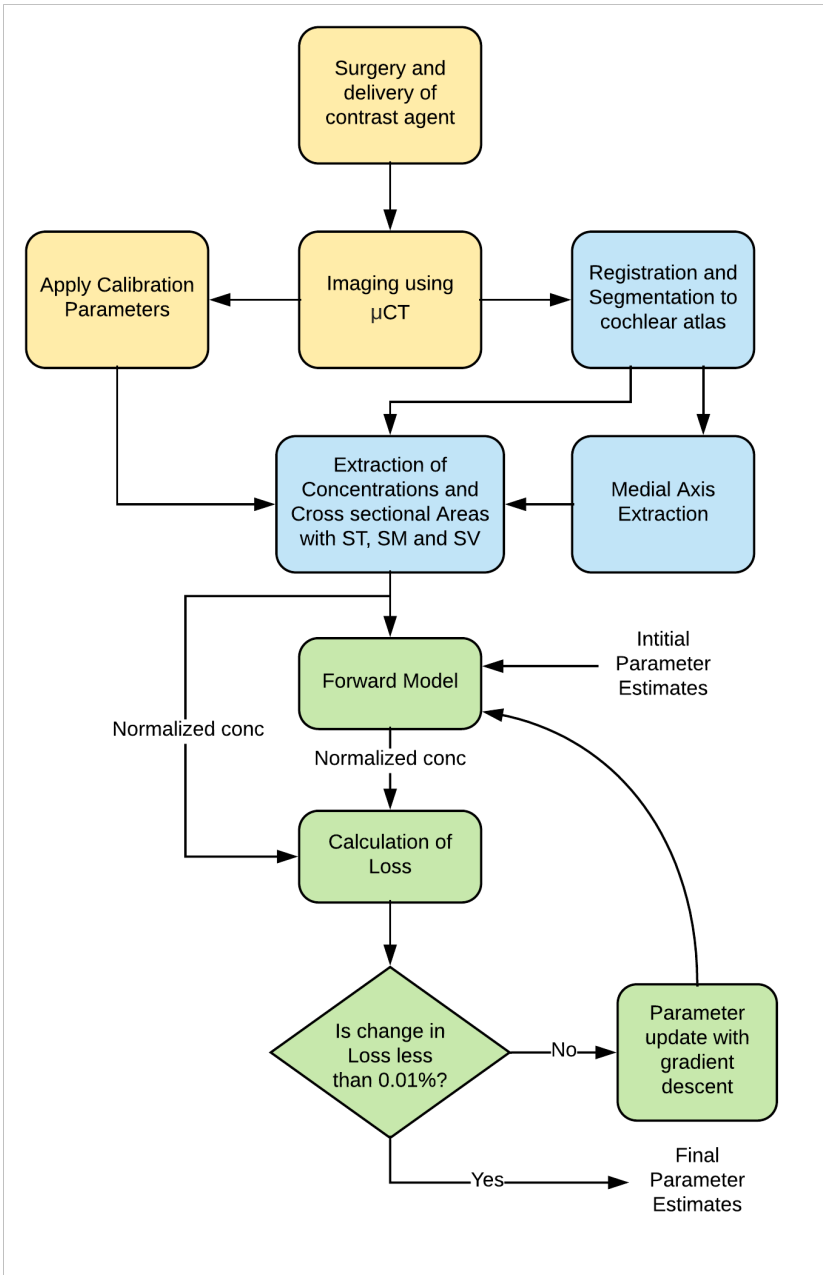

Figure 1: The flowchart gives an overview of the process involved in the extraction of concentrations from the μCT scans and the parameter optimization. Yellow boxes indicate processes involved in imaging the murine cochlea and application of the calibration parameters. Blue boxes represent those processes that involve 3D-Image Processing, which is used to segment the μCT scans and extract the corresponding cross sectional areas and concentration profiles. Green boxes represent the optimization process in which parameters are updated based on the rate of change of loss between the extracted concentrations and the simulated ones generated by the forward model.

2 The inner ear

In his book, William A. Yost describes the structure and function of the ear [15]. The inner ear performs mechanical to neural transduction. The nervous system is provided with information about the frequency, amplitude and temporal content of the sound.

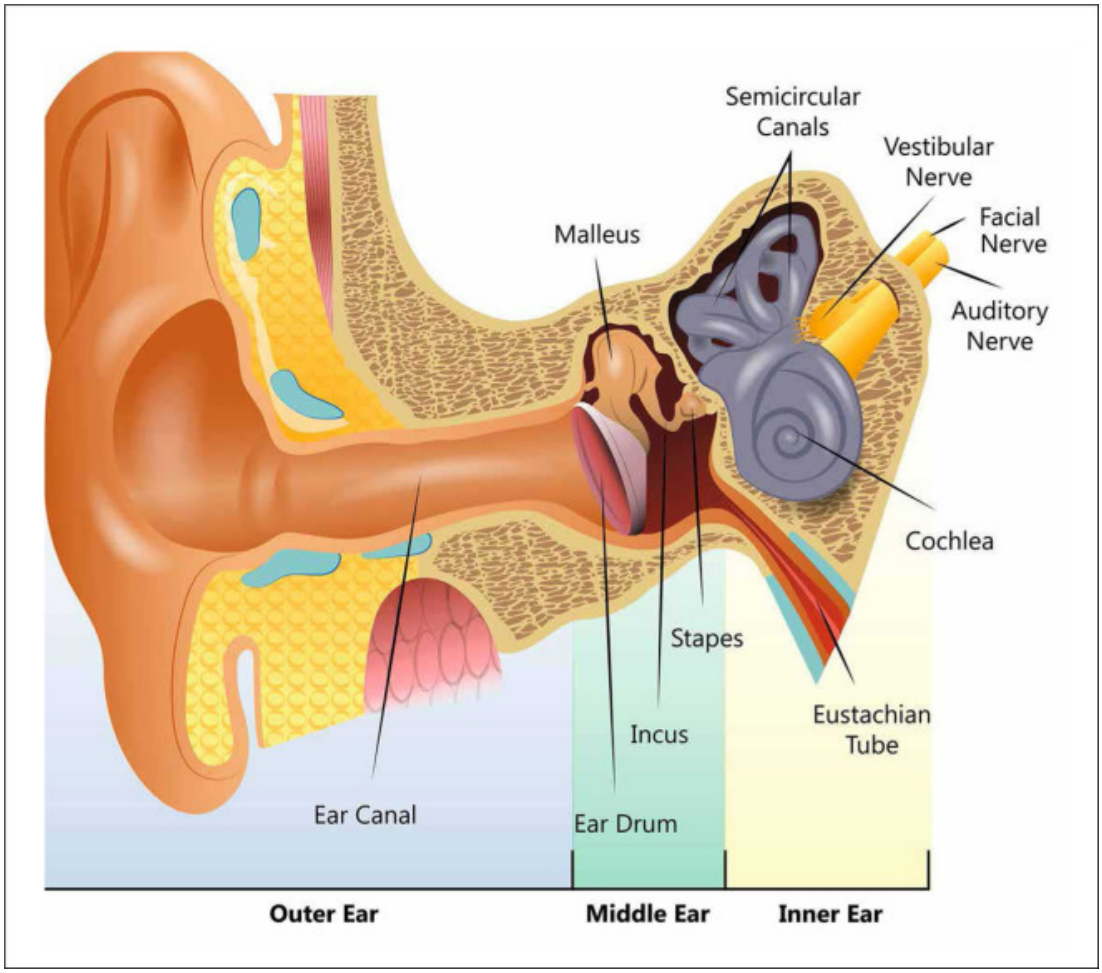

Figure 2: Overview showing the outer, middle and inner ears.
Reproduced from "Microbiology of Middle Ear Infections: Do You Hear What I Hear?" Wolk, 2016, with permission from Elsevier

While our model is based on the mouse, we describe the human cochlea since the differences between them are mostly dimensional and the structure of the ear is similar for most mammals.

The ear is divided into external, middle and inner ears. The external or outer ear includes the pinna, concha and the external auditory canal. The pinna and concha are used to direct sound to the external

auditory canal which ends with the ear drum or tympanic membrane. The ear drum acts as a partition between the external and middle ear. It is connected to the ossicles which are three bones suspended from ligaments in the middle ear. The bones viz. malleus, incus and stapes form the ossicular chain. The stapes is shaped like a stirrup with the footplate implanted in the oval window. The ossicular chain vibrates when stimulated by the vibration of the tympanic membrane, thus causing vibrations in the inner ear through the round window. The inner ear is made up of three parts the semicircular canals, the vestibule and the cochlea. The semicircular canals affect vestibular system. The vestibule is bounded laterally by the oval window. The cochlea is primary auditory organ of the inner ear. Since the sensory units of the auditory and vestibular systems are the hair cells, they are the targets of corticosteroids or regenerative drugs or protective agents. They are housed within the cochlea so an overview of the structure and functioning of the cochlea would aid in illustrating the simplification of the pharmacokinetic model used for the forward and inverse model.

2.1 The cochlea

The cochlea is a spiral tube of bone of decreasing diameter. Along the entire length of the cochlea, a ledge of bone called the Osseous spiral lamina extends out of the modiolus or the central axis of the spiral. The basilar membrane extends out from the spiral ligament and connects to the Osseous spiral lamina, dividing the entire canal except at the helicotrema which connects the scala tympani and scala vestibuli at the apex. The scala tympani (ST) is the lower passage which is separated from the tympanic cavity by the round window membrane (RW). It is connected through a bony channel called the cochlear aqueduct to the subarachnoid space near the brain. The scala vestibuli (SV) is the upper passage which is connected to the tympanic cavity via the footplate and oval window. The Reissner's and basilar membranes enclose a cochlear filled sac with endolymph. The sac is called the scala media (SM). The organ of corti lies on the spiral lamina and the basilar membrane and include an inner tunnel of corti filled with cortilymph which is flanked by inner and outer hair cells. The endolymph within the scala media has a higher concentration of potassium ions than sodium ions, while the scala tympani and vestibule are filled with perilymph that has a higher concentration of sodium ions than Potassium ions. The tips of the hair cells are in contact with endolymph while their bases are in contact with perilymph, the differences in charges and concentrations of the ions between these fluids create a resting (or dc) potential difference between scala media and scala tympani.

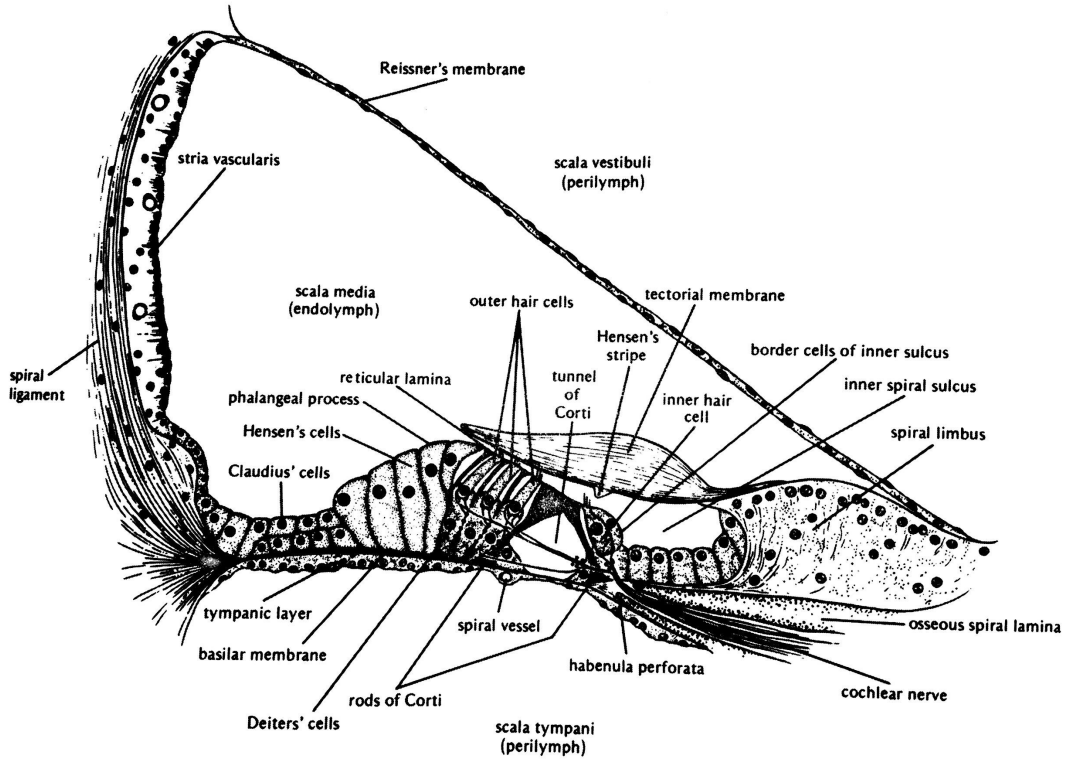

Figure 3: Cross section of the cochlea showing scala tympani (ST), scala media (SM) and scala vestibuli (SV). SV and SM are separated by Reissner's membrane, while ST and SM are separated by the basilar membrane and the organ of corti. The basilar membrane and organ of corti together are important structures in transduction of sound waves to electrical signals. SM is in direct contact with the stria vascularis which is a wall of blood capillaries which is important for transport to the rest of the body.
Reproduced from "Fundamentals of Hearing" 5th Ed., William A. Yost, with permission from Elsevier

2.2 The hair cells

The hair cells have a membrane on their upper surfaces with cuticles in which the bases of smaller 'hairs' or cilia called stereocilia are rooted. Hair cells are located between the tectorial and basilar membrane. On reception of mechanical sound waves, the tectorial and basilar membranes vibrate resulting in shearing forces acting on the stereocelia. The shearing in the cilia on the IHC probably takes place due to movement of the fluids, since their tips are free, while those on the OHC take place due to tectorial membrane movement since their tips appear to be firmly attached to it. Shearing of the stereocila aids in causing ion channels to open and close, transducing mechanical energy into electrochemical activity in the hair cells. This is done by changing the permeability of the hair cell membranes to allow movement of Na+ and K+ ions in and out of the cell. Differences in the concentrations and charge of ions between intra

and extracellular fluids give rise to a potential difference across the cell membrane. Adequate stimulus changes the cell membrane permeability so that Na+ ions can flow in. Even if no stimulus is applied, a potential difference exists across the cell membrane aka resting potential. The resting potential is negative, the flow of Na+ into the cell changes it to a less negative value, i.e. depolarization takes place. Once a critical potential difference is reached, the cell membrane changes permeability at the next point. At the original point, the ions move back their resting state with some undershoot (hyperpolarization). The ion exchanges triggered down the nerve result in the propagation of action potential down the nerve.

Since drugs delivered to the cochlea are directed towards the hair cells, it is important to quantify them to make sure the drug falls within the therapeutic window i.e. the range of values where the benefits of the drug outweigh its toxicity.

3 Pharmacokinetics of the inner ear

How a drug is handled by an organism's body is complex depending on the processes of absorption, distribution, metabolism and elimination. These processes are often simultaneous and may also need to take into account the process of liberation or delivery of the drug. The study of the time course of these processes is referred to as pharmacokinetics.

Simplification of processes is necessary for prediction of drug behavior. This is most commonly done with compartmental models. They are classified based on the number of compartments that are used as an assumption for the model i.e. single, double or multi-compartment models. A single model assumes the organ or subset of organs as being isolated from the rest of the organism's body, this means that a part of an organ or even the entire body can be treated as a single compartment or a single black box. Similarly a double or multi-compartmental model assumes the body is divided into two or multiple black boxes respectively. Our model divides the cochlea into the 3 compartments, the scala tympani, scala media and scala vestibuli, we discuss this in more detail in this section. Solute dispersal processes in this model are a combination of transport processes described within a compartment by diffusion and longitudinal flow, and those describing interscala communications and clearance by permeation [13]. Fluids in the inner ear are fairly stable, and majority of transport takes place via diffusion and permeation. But in the case of a cochleostomy in scala tympani, where the substance is delivered through a hole drilled directly into ST, advection or flow is an important parameter in describing transport, as the substance will flow from the point of delivery out of the cochlear aqueduct which acts like a sink. So we first discuss the governing partial differential equations for diffusion and advection within a tube, followed by permeation (which also describes clearance) along the lines of those described by Hobbie and Roth [16]. Once we combine these cases, we go on to describe our forward 1D model. The units of concentration are in mg/ml (mass/volume) unless specified otherwise.

3.1 Longitudinal Transport: Diffusion and Advection

The process of random movement of particles from a region of higher concentration to that of lower concentration is called diffusion. The particles involved move independently and may collide with those of the solvent but rarely collide with each other at low concentrations. The solvent may be at rest or moving. Fick's first law of diffusion relates the solute flux j or the amount of solute passing through unit area per unit time with the change in concentration $c(x)$ per unit length x. D is the diffusion coefficient or diffusivity in mm^2/s.

$$j = -D\frac{\partial c(x)}{\partial x} \tag{1}$$

Consider a cylindrical tube of certain length, L in the x direction. It has a cross sectional area S. A solution flows through it at velocity v. The concentration of the solution at any point along the length, L is $\bar{c}(x)$ which represents the average concentration across that section. The volume, V over any infinitesimally small length would be Sdx.

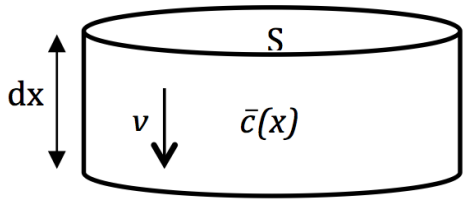

Figure 4: Cylindrical section of length dx and cross sectional area S, with concentration $\bar{c}(x)$ flowing through it at velocity v . The volume of the section, V would be Sdx.

Since we are assuming transport (diffusion and advection) along x, the solution will not be well mixed in this direction. The flux at steady state or dynamic equilibrium would be,

$$j_x = -D\frac{d\bar{c}(x)}{dx} + v\bar{c}(x) \tag{2}$$

For non-steady state diffusion, Fick's second law (for diffusion only) or the diffusion-advection equation needs to be used along the x direction. This is derived from Eqn. 2 using the mass continuity equation

$$\frac{\partial \bar{c}(x,t)}{\partial t} + \nabla j_x = 0 \tag{3}$$

$$\frac{\partial \bar{c}(x,t)}{\partial t} + \nabla\Big(- D\frac{\partial \bar{c}(x,t)}{\partial x} + v\bar{c}(x,t)\Big) = 0 \tag{4}$$

In scalae of small cross sectional areas, it can be assumed the concentration is radially uniform [14], so ∇ can be replaced by $\partial/\partial x$,

$$\frac{\partial \bar{c}(x,t)}{\partial t} + \frac{\partial}{\partial x}(-D\frac{\partial \bar{c}(x,t)}{\partial x} + v\bar{c}(x,t)) = 0$$

$$\frac{\partial \bar{c}(x,t)}{\partial t} - \frac{\partial}{\partial x}\Big(D\frac{\partial \bar{c}(x,t)}{\partial x}\Big) + \frac{\partial}{\partial x}(v\bar{c}(x,t)) = 0 \tag{5}$$

$$\frac{\partial \bar{c}(x,t)}{\partial t} = \frac{\partial}{\partial x}\Big(D\frac{\partial \bar{c}(x,t)}{\partial x}\Big) - v\frac{\partial \bar{c}(x,t)}{\partial x} \tag{6}$$

If D is constant and v is zero, the equation reduces to Fick's second law. We now discuss the conditions when D may not be constant.

3.1.1 Concentration dependent diffusion

The diffusion coefficient of a solute, is a function of the temperature (T), the viscosity of the substance or solvent it is diffusing into (η), and its hydrodynamic radius (r_H). The viscosity and radius together make up the friction factor of the molecule ($6\pi\eta r_H$). If k_B denotes Boltzmann's constant, the diffusion coefficient can be given by the equation below.

$$D = \frac{k_B T}{6\pi\eta r_H} \tag{7}$$

The hydrodynamic radius is representative of the size of each molecule as it diffuses through the solvent. It is directly proportional to the cube root of the molecular weight (MW) of the substance, since the molecular weight itself is considered to be representative of the volume. If ρ represents the density of the pure solute and $\mathcal{N}_0$ is Avogadro's number, then the relation between r_H and MW for a spherical molecule are as given.

$$r_H = \Big(\frac{3MW}{4\pi\rho\mathcal{N}_0}\Big)^{1/3} \tag{8}$$

It can be noted that since viscosity of a solute is a function of concentration, the diffusion coefficient would also change with any changes in concentration. In most experiments, with molecules with low viscosity, these changes can be considered to be negligible. However, in cases where the the viscosity can change rapidly with concentration, this might be a necessary factor to take into consideration. In the absence of a closed form expression between the concentration and viscosity, a substitute relation may

be used.

Fujita provided formal solutions for a modified version of Fick's second law with a concentration dependent diffusion coefficient [17].

$$\frac{\partial c}{\partial t} = \frac{\partial}{\partial x}\left(D(c)\frac{\partial c}{\partial x}\right)$$

subject to

$$c = 0, x > 0, t = 0; c = c_0, x = 0, t > 0$$

where c_0 is the the concentration infused. For the purpose of our model, we made use of one of their provided relations so as to model the concentration dependent apparent diffusion coefficient

$$D(c_{v/v}) = \frac{D_0}{(1-\gamma c_{v/v})^2} \tag{9}$$

While the units of concentration do not matter in the equation as long as its multiplication with γ is unitless, we use $c_{v/v}$ which denotes concentration in terms of volume/volume. This allows us to take into consideration the entire possible range of concentrations from 0 (solution with no solute) to 1 (solution only made up of solute). This is equivalent to D(c), in mass/volume terms as

$$D(c) = \frac{D_0}{(1-\gamma c/\rho)^2} \tag{10}$$

Where ρ is the density of the solute. In this relation, D_0 is the theoretical diffusion coefficient when the concentration of the solution tends to zero, and γ is the factor that decides at what concentration the diffusion coefficient starts to drop off towards zero.

$$D_0 = \lim_{c\to 0} \frac{k_B T}{6\pi\eta(c) r_H} \tag{11}$$

D_0 can be calculated by making use of Eqn 7, by substituting the viscosity of the pure solvent which would represent a concentration of zero. The Eqn 9 is simple and will be able to help us represent a diffusion coefficient that plateaus as the concentration reaches 0 as well as when it reaches 1, in a manner similar to a sigmoid curve.

3.1.2 Diffusion and Advection in a tube of varying Cross sectional area

Clifford S. Platak in his paper [18] derived Fick's second law for diffusion within a long tube. We extend this derivation to include a non constant diffusion coefficient as well as fluid flow through the tube. Consider a thin tube of varying cross section S(x), such that its length is much longer than its cross sectional area or radius at any point. Again we assume the concentration across a cross section to be well mixed at all instances. The solution is considered to be incompressible and flowing into the tube at a volumetric flow rate $F(t)$ resulting in a velocity of the fluid $\bar{v}(x,t)$ at each point along the length, where $\bar{v}(x,t) = F(t)/S(x)$. Similar to the mass-continuity equation in 3, we start with the equation below

$$\frac{\partial}{\partial t}\iint_{S(x)} c(x,y,z,t)\,dS = -\frac{\partial}{\partial x}\iint_{S(x)} j_x(x,y,z,t)\,dS \tag{12}$$

Since the diffusion coefficient is concentration dependent, it can also be considered to be a function of space and time. So the above equation can be rewritten as

$$\frac{\partial}{\partial t}\iint_{S(x)} c(x,y,z,t)\,dS = -\frac{\partial}{\partial x}\iint_{S(x)} \Big[-D(x,y,z,t)\frac{\partial c(x,y,z,t)}{\partial x} + v(x,y,z,t)c(x,y,z,t)\Big]\,dS \tag{13}$$

This reduces to

$$S(x)\frac{\partial \bar{c}(x,t)}{\partial t} = \frac{\partial}{\partial x}\Big[\bar{D}(x,t)S(x)\overline{\frac{\partial c(x,t)}{\partial x}} - S(x)\bar{v}(x,t)\bar{c}(x,t)\Big] \tag{14}$$

Since the assumption has been made that the solution is well mixed across cross sections,

$$\frac{\partial \bar{c}(x,t)}{\partial x} = \overline{\frac{\partial c(x,t)}{\partial x}}$$

Also $\bar{D}(x,t) = D(\bar{c}(x,t))$, which we will henceforth denote as $D(x,t)$, reducing the equation to

$$\frac{\partial \bar{c}(x,t)}{\partial t} = \frac{1}{S(x)}\frac{\partial}{\partial x}\Big[D(x,t)S(x)\frac{\bar{c}(x,t)}{\partial x} - S(x)\bar{v}(x,t)\bar{c}(x,t)\Big] \tag{15}$$

$S(x)\bar{v}(x,t)$ can be replaced with $F(t)$, so the final form of the equation will be

$$\frac{\partial \bar{c}(x,t)}{\partial t} = \frac{1}{S(x)}\frac{\partial}{\partial x}\Big[D(x,t)S(x)\frac{\bar{c}(x,t)}{\partial x}\Big] - \frac{F(t)}{S(x)}\frac{\bar{c}(x,t)}{\partial x}, \quad 0 \le x < L \tag{16}$$

$$\frac{\partial \bar{c}(L,t)}{\partial x} = 0, x = L$$

$$\bar{c}(x,0) = \bar{c_0}(x), t = 0$$

This PDE represents longitudinal transport within a tube of varying cross sectional area.

3.2 Transport across a membrane: Permeation

A semi-permeable membrane allows only certain substances to pass through it, so while perilymph and endolymph do not pass through the membranes within the cochlea, some contrast agents and drugs delivered into those regions do. The motion of the solute molecules are not independent of those of the solvent, since the fluids in the inner ear are at rest, movement between compartments also take place via diffusion. In such cases the transport is referred to as permeation and in this case the solute flux is proportional to the intercompartmental concentration gradient

$$j \propto \Delta c \tag{17}$$

$$j = \omega RT\Delta c \tag{18}$$

Where ω is the membrane permeability, R is the ideal gas constant and T is the temperature in Kelvin. Since we are only concerning ourselves with the term collectively, we will denote it as the transfer coefficient K.

$$j = K\Delta c \tag{19}$$

Clearance refers to the removal of the drug or contrast agent from the organ. Clearance in our model is represented by the transfer coefficient of the membrane between the scala media and the stria vascularis. While clearance is usually represented by transport out of spiral ligament (SL) to blood, we consider clearance directly out of scala media due to the limitations in extracting concentrations out of SL. This is possible since SL in the mouse is mostly in contact with SM and has very little contact with ST and SV.

We now take into consideration two cylindrical compartments with volumes V and V' and concentrations $\bar{c}(x,t)$ and $\bar{b}(x,t)$ with transport between them occurring through a membrane of area A. The concentration in each section of length dx is considered to be radially uniform. This means that at each point along x, the concentration is well mixed across the cross sectional area S, or instantaneous mixing occurs across the cross section when any change in concentration occurs at any point within it.

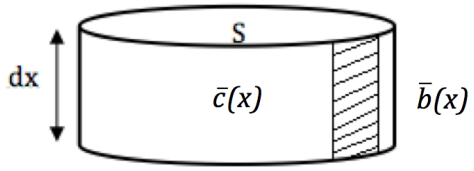

Figure 5: Cylindrical section of length dx and cross sectional area S, with concentration $\bar{c}(x,t)$ at time t. The section has a semipermeable membrane of area A in contact with another compartment of concentration $\bar{b}(x,t)$. The volume of the section, V would be Sdx.

The flux in the y direction would be

$$j_y = -K(\bar{c}(x,t) - \bar{b}(x,t)) \tag{20}$$

Where K depends on the physical properties of the membrane such as thickness, pore size and density, and its units are in mm/s.

Representing the flux j_y in terms of the number of moles N_y,

$$\frac{\partial N_y}{A(x)\partial t} = -K(\bar{c}(x,t) - \bar{b}(x,t)) \tag{21}$$

$$\frac{\partial N_y}{\partial t} = -KA(x)(\bar{c}(x,t) - \bar{b}(x,t)) \tag{22}$$

Dividing both sides by the volume of the section, V(x)

$$\frac{\partial N_y}{V(x)\partial t} = -\frac{KA(x)}{V(x)}(\bar{c}(x,t) - \bar{b}(x,t)) \tag{23}$$

$$\frac{\partial \bar{c_y}(x,t)}{\partial t} = -\frac{KA(x)}{V(x)}(\bar{c}(x,t) - \bar{b}(x,t)) \tag{24}$$

It can be seen that the change in the number of moles of the substance is independent of the volume it is in and is only dependent on the area of the membrane it is trying to permeate out of and the concentration gradient between the compartments. This is due to the fact that irrespective of the size of the compartments, permeation will take place till the solute is equally dispersed throughout both compartments i.e. their concentrations are equal.

These equations for transport in the x and y directions can be combined to model transport as a whole.

3.3 Combined model for Diffusion, Advection and Permeation

We now consider a model with all three modes of transport; concentration dependent diffusion, advection and permeation through a tube of varying cross sectional area. The figure shows a single infinitesimal section taken into consideration. The length of the whole tube is L and the initial concentration is $\bar{c_0}(x) = \bar{c}(x,0)$.

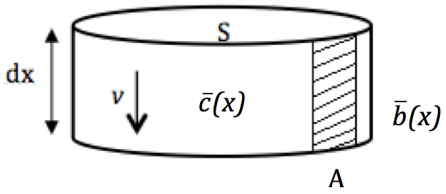

Figure 6: Cylindrical section of length dx and cross sectional area S, with concentration $\bar{c}(x,t)$ flowing through it at velocity v. Permeation takes place through a semi-permeable membrane of area A to a section of another compartment of concentration $\bar{b}(x,t)$. The volume of the section, V would be Sdx. Diffusion takes place in the x direction while permation takes place across y.

From equations 5, 16 and 24, we get the final form of the partial differential equation $\partial c/\partial t = \partial c_x/\partial t + \partial c_y/\partial t$

$$\frac{\partial \bar{c}(x,t)}{\partial t} = \frac{1}{S(x)}\frac{\partial}{\partial x}\Big[D(x,t)S(x)\frac{\partial \bar{c}(x,t)}{\partial x}\Big] - \frac{F(t)}{S(x)}\frac{\partial \bar{c}(x,t)}{\partial x} - \frac{KA(x)}{V(x)}(\bar{c}(x,t) - \bar{b}(x,t)), \quad 0 \le x < L \tag{25}$$

$$\frac{\partial \bar{c}(L,t)}{\partial x} = 0, x = L$$

$$\bar{c}(x,0) = \bar{c_0}(x), t = 0$$

3.4 Our Model

A representation of the reduced model we use is given in the following figure. Scala tympani, and scala vestibuli are considered to have transport only with scala media. Clearance to blood takes place out of the spiral ligament, but we have low confidence in the concentrations extracted from the spiral ligament. The plots tend to be noisy since the registered labelmap is very thin, which is prohibitive for the extraction. Instead, we treat the spiral ligament as a membrane itself, so SM is considered to clear out to blood in the scala vascularis. The semipermeable membranes between scalae, (Basilar membrane between ST and SM, and Reissner's membrane between SV and SM) as well as transport between SM and blood via the

stria vascularis are represented by dashed lines. Solid lines represent bone or the inability for transport to take place out of the scala through that boundary. Contrast agent will be delivered at a certain flow rate

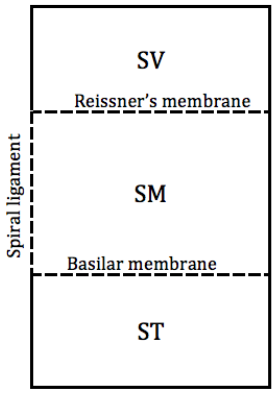

Figure 7: Cross section of our 1D model, diffusion and advection are considered to take place in a direction perpendicular to the plane of the page. Dashed lines represent transport between scalae, solid lines represent no transport

at the base of ST. The contrast agent flows out of the cochlear aqueduct, resulting in the point of delivery acting like a constant source. Over time, the agent diffuses down the length of ST and up into SM and SV. So from the point of delivery upto the apex, equation 25 reduces since $v = 0$, and from the point of delivery down to the cochlear aqueduct, the equation will be used as is.

If x_0 is the point of delivery, then the PDE governing transport from x_0 to the apex will be

$$\frac{\partial \bar{c}(x,t)}{\partial t} = \frac{1}{S(x)}\frac{\partial}{\partial x}\Big[D(x,t)S(x)\frac{\partial \bar{c}(x,t)}{\partial x}\Big] - \frac{KA(x)}{V(x)}(\bar{c}(x,t) - \bar{b}(x,t)), \quad x_0 < x < L \tag{26}$$

$$\frac{\partial \bar{c}(L,t)}{\partial x} = 0, x = L$$

$$\bar{c}(x,0) = \bar{c_0}(x), t = 0$$

The PDE for transport from the point of delivery down to the base in ST will be

$$\frac{\partial \bar{c}(x,t)}{\partial t} = \frac{1}{S(x)}\frac{\partial}{\partial x}\Big[D(x,t)S(x)\frac{\partial \bar{c}(x,t)}{\partial x}\Big] - \frac{F(t)}{S(x)}\frac{\partial \bar{c}(x,t)}{\partial x} - \frac{KA(x)}{V(x)}(\bar{c}(x,t) - \bar{b}(x,t)), \tag{27}$$

$$0 < x \leq x_0$$

$$\frac{\partial \bar{c}(0,t)}{\partial x} = 0, x = 0$$

$$\bar{c}(x,0) = \bar{c_0}(x), t = 0$$

Equation 26 equated within each scala, will be used for the inverse model to learn the permeability coefficient for each membrane, while 27 will be equated at the point of delivery, to learn the flow rate and leakage rate during delivery.

3.5 Translating transport coefficients to a different solute

Given the theoretical diffusion coefficient of a solute when its concentration is zero (D_0) or the permeation coefficients, they can be scaled for other compounds using the simple relation mentioned in Eqn 7. The ratios of the D_0 of each compound can be given by

$$\frac{D_{0new}}{D_{0old}} = \frac{r_{Hold}}{r_{Hnew}} \tag{28}$$

This can further be simplified using Eqn 8

$$\frac{D_{0new}}{D_{0old}} = \sqrt[3]{\frac{MW_{old}\rho_{new}}{MW_{new}\rho_{old}}} \tag{29}$$

We also consider the case of permeation at the membrane and treat it like diffusion across it in the y-direction, we alter Eqn 1, for the case of permeation to get

$$j_y = -D\frac{\partial c}{\partial y} \tag{30}$$

This could be discretized to give us

$$j = \frac{-D\Delta c}{\Delta y} \tag{31}$$

This can be compared to Eqn 19 so that

$$K = \frac{-D}{\Delta y} \tag{32}$$

This means that the permeability coefficient can be treated as the ratio of coefficient of diffusion of a solute within that membrane to the thickness of the membrane. Which implies that once the permeability coefficient is found for a certain solute through a certain membrane, it can be scaled using the relation in

29 similar to the case of D_0 above.

$$\frac{K_{new}}{K_{old}} = \sqrt[3]{\frac{MW_{old}\rho_{new}}{MW_{new}\rho_{old}}} \tag{33}$$

So the scaling factor based on the molecular weights and densities of the solutes can be used as a simple method to translate the transport parameters from one molecule to another. However, in the case of the permeation coefficients, this method does not take into account the possibility of a change in interaction of the molecules with the membrane structure. Also, for the diffusion coefficient, we consider γ to be the same for the new molecule, this method assumes that the new molecules also behave in a manner similar to the old solute. For instance, as new solute is pumped into the solution, its viscosity at 10% v/v of the solution is assumed to be the same as the viscosity at 10% of the old solution, which may be inaccurate.

4 Quantification of compounds delivered

An important process in quantification of the contrast agent is sampling, which in our case is done using three dimensional micro-computed tomography (μCT). While the scans provide a volumetric representation of the cochlea, it needs to be segmented based on anatomy so that sampling from the different scalae becomes possible. Segmentation of medical images is problematic due to low contrast and fuzzy contours. For instance, cross sections of thin structures like Reissner's membrane are not visible in the μCT scans used for our experiments. A solution is to use a reference image and register it to the images that we wish to segment [9]. The resulting transformation can be applied to the corresponding labels of the reference image so that segmentation can be achieved by performing registration. Once segmented, the transformed labelmaps can be used to extract the medial axes so that when superimposed on the μCT scans, extraction of intensity values and thus proportional concentrations along the length of the cochlea is possible.

4.1 Drug infusion setup

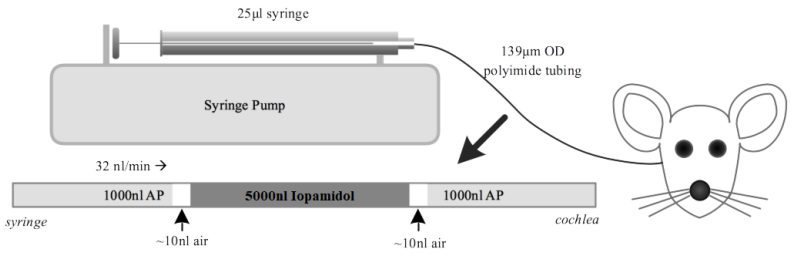

Figure 8: Setup for drug delivery to the mouse cochlea. A volume of 5000nl of Iopamidol (Isovue) is delivered. The air bubbles between the volumes of Artificial Perilymph (AP) and Iopamidol prevent their mixing and also provide a visual reference to ensure the rate of flow through the tube.

The work in this section was performed by the team of Doctors at University of South Florida in a manner similar to that explained by Borkholder et. al [19]. Surgery was performed on the left ears of deeply anesthetized young adult CBA/CaJ mice. A cochleostomy was drilled by hand close to the cochlear aqueduct. The polymide infusion tube was inserted using a micromanipulator and fixed in place using

dental cement. The mice remained anesthetized during the experiment.

Iopamidol, an iodine based contrast agent, and Artificial perilypmh were delivered through the polymide tube connected to a 25μL syringe which was mounted in a syringe pump. Solutions of Iopamidol and artificial perilymph were separated by 10nL air bubbles which helped avoid diffusion of the solutions within the tube and were also used as a visual guide for the flow rate.

4.2 Imaging

The work in this section was performed by the team of Doctors at University of South Florida. The formation of CT images relies on the differential attenuation of photons in body tissue defined by linear attenuation coefficients resulting in the production of contrast in CT images. To improve visibility, contrast agents with high attenuation constants are usually used in experiments. We use Iopamidol, an iodine based contrast agent. Inner ear drug concentrations can be quantified over time for a given infusion protocol, by using an established relation between the image intensity and the concentration of bound iodine in an Iopamidol solution.

A Seimens Inveon scanner was used for the experiments. Each resulting scan is of size $1024 \times 1024 \times 512$ with each voxel of size $16 \times 16 \times 16$ μm. Each full scan takes 20 min to complete, along with a setup time of 10 min between each scan. So scans were taken every 30 min while the infused volumes were recorded manually until the entire volume of Iopamidol was delivered, which was a total of 5 scans during delivery with one more scan being taken before delivery as our baseline scan. The files from each scan were saved as uint16 DICOM images by the scanner. Further processing was performed on these files.

4.3 Calibration

The work in this section was based on work by Haghpanahi et. al [9] and was performed by S. S. Moudgalya. Intensities of μCT scans are quantified in Hounsfield units (HU). The transformation between the attenuation coefficients of air and water at STP are defined such that radio density of air is 0HU and of distilled water is -1000HU. To determine the relationship between the Hounsfield units from the μCT scans and the concentrations of the contrast agent, plastic tubes containing solutions of Iopamidol with concentrations of organically bound Iodine ranging from 0mg/ml (i.e. saline) to 325mg/ml were imaged. A circular region of interest around 80 pixels in diameter was used in each image region with a distinct concentration to calculate the mean and standard deviation of the intensities. The HU intensities were plotted

against the known concentrations and linear regression was used to find the relation between them. The relation found between HU values (y) and concentration of bound Iodine in Iopamidol (x) is given by $y = 29.4133x - 53.1569$. It should be noted that x is not the true concentration of the agent in the solution but the concentration of the bound Iodine in the solution that can be captured by the μCT. Based on the physical properties provided for the compound, multiplying this value with a simple scaling factor of 2.04 will give us the true concentration of the solution.

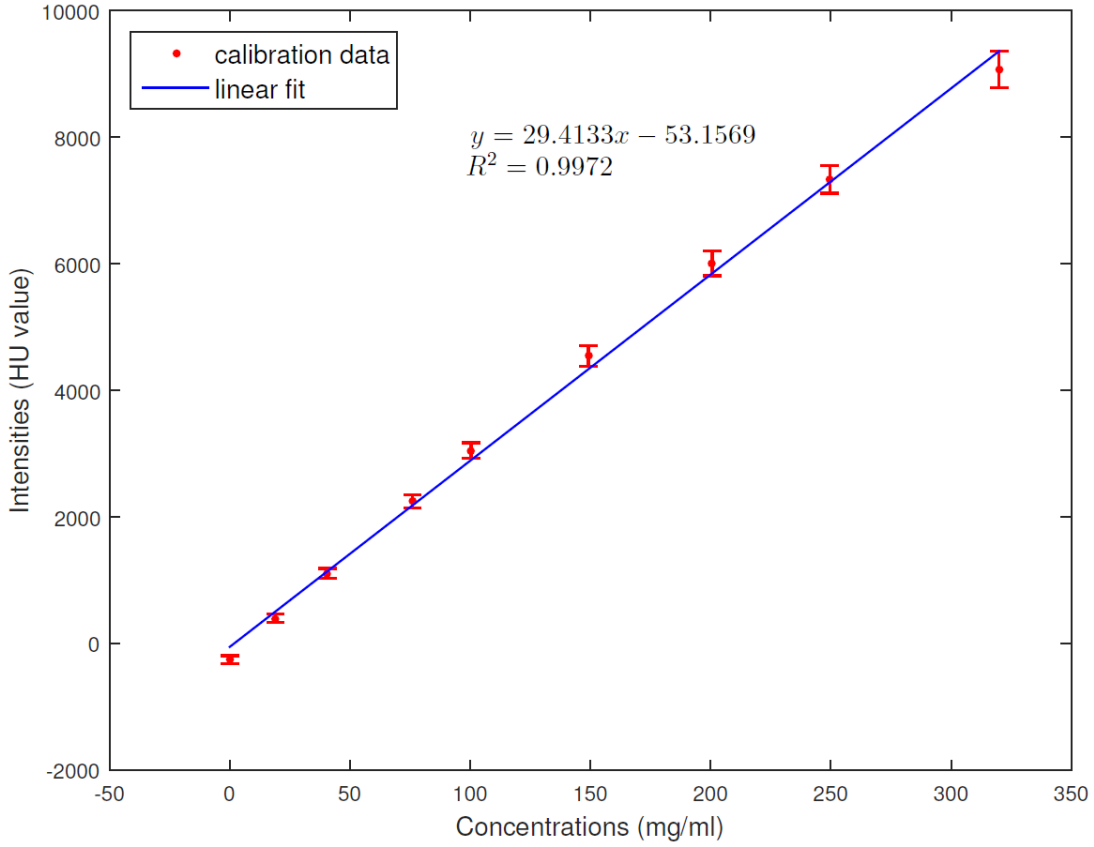

Figure 9: Line fit to the calibration data. HU values are represented by y and concentration of organically bound Iodine in Iopamidol are represented by x.

The image was also used to determine the sensitivity of the μCT machine. The standard deviations of the intensities were converted to the standard deviations of the Iodine concentrations in Iopamidol (σ_c) and a graph of the ratio of noise to the bound Iodine concentration (σ_c/C) was plotted against the bound Iodine concentration (C). A power curve ax^b was fit to the data points and the sensitivity was defined at the point where σ_c/C=1, which falls around 2.6553mg/ml. Changes in Iopamidol less than this

amount may be treated as noise. Based on averages taken in a circular window in the calibration scans for diameters ranging from 1 to 15, we found that a diameter of 5 voxels and above gave variations in average which was lower than the sensitivity value. However, there is no closed form equation for sensitivity and diameter values. A diameter of 7 voxels was chosen since it is large enough to ensure that the variations were lower than the sensitivity and small enough that we do not overlap any bone in apical regions during extractions.

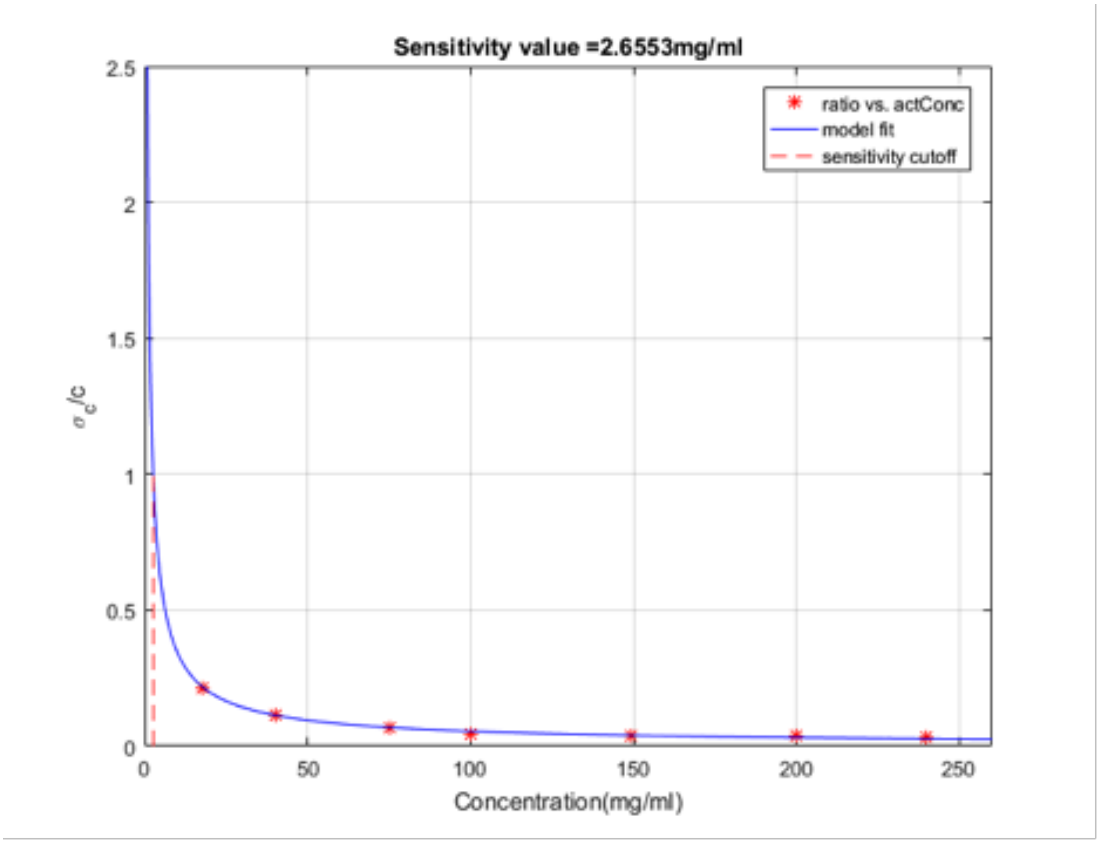

Figure 10: Plot of σ_c/c vs c where c represents concentration in mg/ml and σ_c represents the standard deviation of the concentration of bound Iodine. The sensitivity cut off is at 2.6553mg/ml with concentrations lower than this being treated as noise.

4.4 Registration and Segmentation

The work in this section was based on initial work by X. Zhu [20] with significant modifications by S. S. Moudgalya. Despite having high resolution, segmentation of medical images is problematic due to low contrast, blurry contours and similar intensities for adjacent objects of interest. With the use of a reference

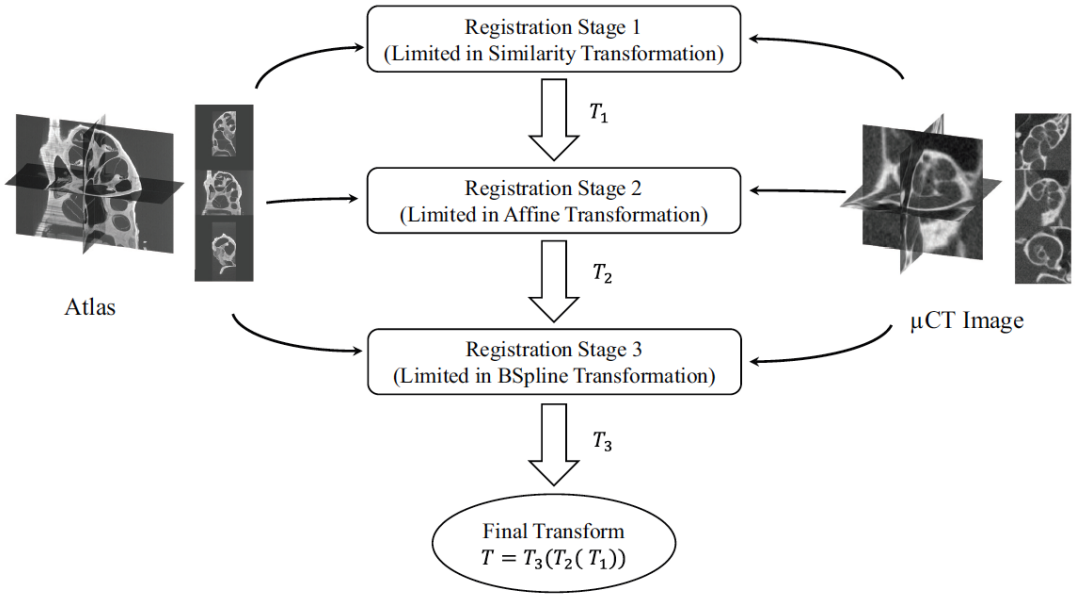

Figure 11: Multistage registration is performed by registering the same set of scans at different resolutions

image and labelmaps as apriori knowledge, segmentation can be reduced to registration by applying an equivalent transformation to the atlas labels. This is done by solving a problem to optimize the similarity metric. A similarity metric is used to determine how well the moving image is registered to the fixed image. We make use of Mutual information as the similarity metric which is the difference between the sum of the individual entropies and the joint entropy.

$$\mathscr{I}(A,B) = H(A) + H(B) - H(A,B) \tag{34}$$

Scans of the entire mouse head are taken so a region of interest (ROI) can be determined manually. Once determined for the baseline scan the same voxel indices can be used for the remaining scans assuming there is no movement of the mouse between scans. In case of movement between scans, an ROI of the same size but a different origin is determined and the atlas is registered to each of the scans so that at the end of the process each scan has a corresponding labelmap. We make use of Santi's mouse cochlea database [10] as our atlas. They consist of 2D image stacks of histology slices taken at 20μm spacing from each other and with each slice of $5.453 \times 5.453\mu$m resolution.

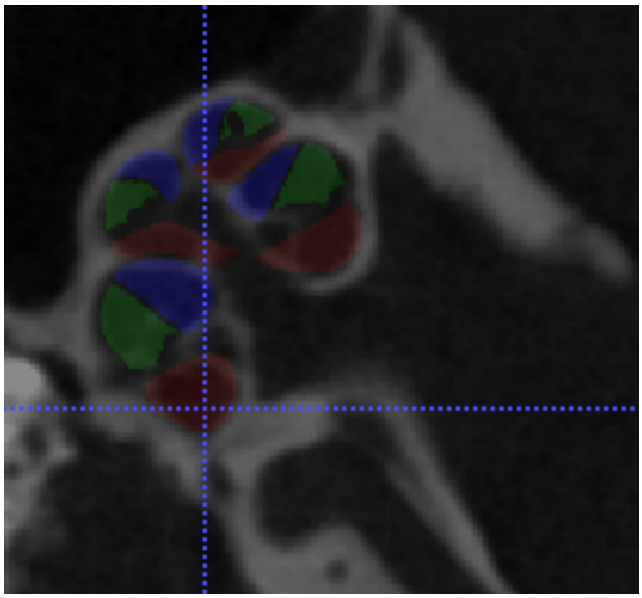

Figure 12: An example of the results of a segmented mouse cochlea. The red regions represent ST, green SM and blue SV. The greyscale regions represent bony and membranous structures.

For registration, a combination of multi resolution and multi stage strategies are used. Images that have been decimated by factors of 3 and 2 are used for rigid transformations of similarity and affine stages where the image is rotated and scaled. The original atlas resolution is used for deformable registration where splines are fit to try and deform the image locally. The transformations can be treated as a cascade of systems and the resulting transform is applied to the labelmap.

4.5 Medial Axis extraction

Apart from the concentrations, the rate of diffusion within and between compartments depends on their physical dimensions. Our model calls for the use of cross sectional areas along the length of each scala. To aid in the extraction of concentrations as well as the cross sectional areas, the medial axis or skeleton is required. The medial axis of a structure is the locus of centers of maximally inscribed hyperspheres. Medial axis extraction is also referred to as skeletonization. Kerschnitzki, Kollmannsberger et al developed a MATLAB plugin [21] based on a skeletonization work by Lee et al. [22], which describes the work given in this section.

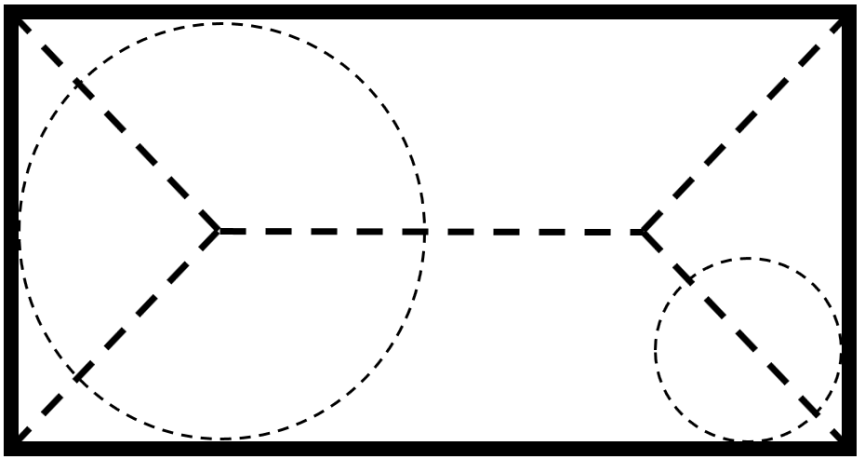

Figure 13: 2D example of a rectangle with inscribed hyperspheres whose centers form the skeleton

4.5.1 Digital Topological requirements

We consider an 'object' made up of S, a set of voxels (volume elements) with value 1, with 26-connectivity in a binary 3D space, where each voxel p is represented by its centroid (i,j,k). The remaining voxels, with value zero in the space $\bar{S}$ are considered to be the background. For the extraction of the medial axis, voxels need to be removed from the set S or its value set to zero. The removal of a voxel p must preserve the topology of the space i.e. the number of objects $O(S)$, the number of holes $H(S)$ and the number of cavities $C(S)$ must remain the same. While objects are considered to be distinct disconnected subsets of voxels, cavities are empty spaces completely surrounded by S and holes are like tunnels i.e. not completely surrounded by S (like donuts). However holes can be difficult to define in 3D, and the checking of global conditions for the removal of every point is computationally expensive. To help overcome these issues certain conditions have been put forward.

4.5.1.1 Global and local Euler Formula The Euler characteristics help define a 3D hole consistently. The Euler characteristic $\chi(S)$ is given by

$$\chi(S) = O(S) - H(S) + C(S) \tag{35}$$

Where $O(S)$ is the number of objects, $H(S)$ is the number of holes and $C(S)$ is the number of cavities in S. To reduce the complexity, a local Euler formula $G(S)$ can be used where

$$\chi(S) = \sum_i G(S \cap N(p_i)) \tag{36}$$

$$G(S) = v - e + f - oct \tag{37}$$

where v, e, f and oct are the number of vertices, edges, faces and octants, within S, and $N(p_i)$ is a $3 \times 3 \times 3$ neighborhood around voxel p_i and $p_i \epsilon S$.

4.5.1.2 Simple Border Point A point or voxel in S is considered to be a border point if it is 6-connected to a voxel in $\bar{S}$. 'Simple' points have often been used in thinning operations for the purpose of preserving topological conditions. A border point (p) is simple if and only if the number of connected objects and holes for S and $\bar{S}$ do not change on removal of the point. These points have been shown to have the following properties

$$\begin{aligned} \delta G(S \cap N(p)) = 0; \quad & and \\ \delta H(S \cap N(p)) = 0; \quad & or \\ \delta O(S \cap N(p)) = 0 & \end{aligned} \tag{38}$$

where δ denotes the change in the neighborhood on removal of the point. Also, since the 26 neighbors of p are connected to it, $O(S \cap N(p))$ is always 1 before removal of p. So if removal of p causes $O(S \cap N(p))$ to remain 1, we have

$$\delta O(S \cap N(p)) = 0 \text{ if and only if } O(S \cap N(p)) = 1 \tag{39}$$

The above conditions can be used to test simplicity.

4.5.2 Parallel Thinning Operations

While only simple border points of an object need to be deleted for the purpose of medial axis extraction, these operations need to be performed in parallel. This may result in instances where with the sole use of these criteria, deletion of a point may lead to deletion of the entire object. A common way to eliminate the problem is dividing each thinning operation into 6 subcycles in a fixed order, depending on the type

of simple border point in consideration, and checking for preservation of connectivity before and after removal of such points. The type of a simple border point is based on its 6-connectivity to the remaining voxels in the neighborhood i.e. up (U), bottom (B), north (N), south (S), west (W), east (E). If R is considered to denote a set of simple border points of a certain type, and $Q = S - R$, each of those points is examined for path connectivity; p is only removed if voxels in $Q \cap N(p)$ and $R \cap N(p)$ remain connected after its removal ($O(\{R \cap N(p)\} \cup \{Q \cap N(p)\}) = 1$). To extract the medial surface or the medial axis, border points of S are repetitively deleted if they satisfy the above conditions until no more points can be removed. More geometric constraints can be added based on whether a medial surface or a medial axis needs to be extracted. But since a medial axis is usually extracted from a medial surface, we first provide the conditions for the extraction of the surface.

In medial surface thinning, the object is thinned so that its thickness is one voxel in any one of the three principal directions of a plane. Given an octant ($N^2(p)$), a plane can be considered to run through it if any 4 vertices lie on a plane (or the points on any 2 parallel edges are all 1, and the rest are 0). This can be done by ordering the vertices of the cube and noting the configuration based on which points are 0 and 1 as indexes in a look up table. Only a small subset (D) of the 2^8 configurations will denote such planes. Apart from this, the point can also be a surface end point where instead, it can be considered that the octant has less than three points set to 1. So a point p is a surface point if $\forall i, i \epsilon \{1,...,8\}$

$$Index[N^2(p_i)] \epsilon D; \quad or \qquad (40)$$
$$|N^2(p_i)| < 3$$

The configuration number is represented by $Index[N^2(p_i)]$, and $|N^2(p_i)|$ denotes the number of set voxels in $N^2(p_i)$. As discussed earlier, medial axis thinning extracts lines and arcs through the center of S instead of a surface. A final condition to consider is used to prevent the removal of the end points. After the removal of all border points of a certain type, at least 2 points need to remain within the neighborhood ($|Q \cap N(p)| \geq 2$).

Let T represent the skeletonization operation with a set order of directions(U, B, N, S, W, E), then T repetitively deletes simple border points from S simultaneously while satisfying these 4 conditions.

($C1$) $\delta G(S \cap N(p)) = 0$

($C2$) $O(S \cap N(p)) = 1$

(*C*3) $O(\{R \cap N(p)\} \cup \{Q \cap N(p)\}) = 1$, where R is the set of border points that satisfy the first two conditions C1 and C2 and $Q = S - R$

(*C*4) (i) p does not meet the surface end point condition, $|N^2(p_i)| \geq 3$, or

(ii) $|Q \cap N(p)| > 1$ where $|Q \cap N(p)|$ is the number of points in $Q \cap N(p)$

The process is continued until no such points are left.

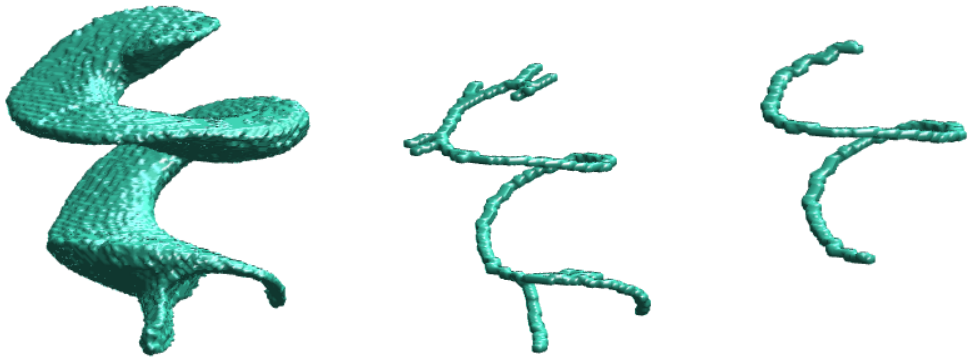

Figure 14: An example illustrating the process of medial axis extraction of the labelmap of scala tympani. The first image shows the original labelmap, followed by what it looks like after the axis is extracted along with all the branches. The final images shows the pruned medial axis which the only part of the original axis we need.

4.5.3 Pruning

Since the input object is noisy, the resulting skeleton contains multiple spurious branches that need to be pruned. To do this, we manually fix the start and end points E and get rid of all other end points iteratively until only the main 'trunk' of the skeleton remains. An end point would be such a point that is connected to only one other point indicating that it is the tip of a branch.

If p $\notin$ E,

Remove p if |N(p)|<3

The process is continued until no such points are left. The condition removes a voxel if there are only two voxels in the neighborhood of p (one more voxel apart from itself). The condition works well when

the extracted skeleton is of single voxel thickness and has no loops, which is usually the case since the labelmaps are open ended. In some instances where the labelmap becomes flatter like towards the apex of a scala, the skeletonization may result in a loop. This issue can be solved with some manual intervention where a voxel form an unwanted branch of the loop is set to zero; essentially disconnecting it and turning it into an open branch. The pruning condition can be run on this structure once more till the single axis is achieved.

For ST, the labelmap branches off into two small structures near the round window membrane as seen in Fig 14. The resulting skeleton has branches near the round window membrane. This point which is located near the cohclear aqueduct is set as the basal end point (or 0%) for ST. Similarly, in SM, we select the basal end point to be the point closest to the RWM in ST; this occurs at a point where it takes a sharp turn to wrap around the basal end of ST. The base point for SV is selected to be the point closest to the oval window membrane. We chose these basal end points since we are not interested in transport that occurs from these points out to the apex. The apical end points for all the scalae were selected as the last points of the medial axes at the apex.

4.5.4 Reparameterization of the Medial Axis

To find the cross sectional areas and average concentrations at each point, we need to know the tangent and normal vectors at those points along the length of the axis. Though the axis is smoother after the removal of of the extra branches of the skeleton, the resulting medial axis is in the discrete space. We can consider a tangent as the vector from one voxel on the medial axis to its neighbor, but this would mean that only 26 directional vectors can be defined (one for each possible neighbor). This could result in the extraction of cross sectional planes that have a large angular displacement from the true cross section at than point, giving us erroneous extractions. Smoothing of this reduced axis is performed by reparameterizing the points in terms of arclength, which means that the coordinates of the points are each treated as functions of the length of the medial axis, $x = f(l)$, $y = g(l)$ and $z = h(l)$, where l is the length. Cubic splines are fit to these points so the curves can be smoothed and the required number of points are uniformly sampled from these curves (100 points in our case). The tangents can be calculated by the first order differentials of these functions, so that they are not limited directionally.

4.6 Extractions of Concentrations and physical dimensions

Concentrations can be extracted along the axis in a couple of ways, planar and volumetric. The first being across the cross section of the plane normal to the tangent at each point; the second is in a sphere around each point. The planar extraction is more accurate but can be susceptible to errors in the direction of the tangent. Small changes in the direction may result in larger shifts in the position of the plane as we move further away from the point in consideration. This susceptibility may not be problematic when we consider small regions for concentration extractions. This process is also important for the extraction of cross sectional areas. While being computationally less expensive, the volumetric extraction is less accurate since it acts like a smoothing filter along the length of the axis.

4.6.1 Planar Extraction

To describe a plane at each of these points, the unit tangent vectors (T) are calculated from the first order derivatives. The second order derivative can be used for the unit normal vectors (N). The cross product of the tangent and normal results in a unit vector perpendicular to both of them and can be called the unit binormal vecotr (B). These sets of 3 vectors at each point can be used to generate a transformation matrix so that the normal and binormal are the principal axes (x and y) in the plane we are considering and the tangent points out of it.

$$[N|B|T]'Tr = I \tag{41}$$

$$Tr = ([N|B|T]')^{-1} \tag{42}$$

However using the transformation matrix directly may give rise to holes as there may be many to one mappings of voxel (to pixel) coordinates. Instead of transforming the plane to a new space, a planar grid of points is set up and the position of these points is calculated in the original space $[x_{old} \quad y_{old} \quad z_{old}]$.

$$\begin{bmatrix} x & y & 0 \end{bmatrix} Tr^{-1} = \begin{bmatrix} x_{old} & y_{old} & z_{old} \end{bmatrix} \tag{43}$$

The coordinates $[x_{old} \quad y_{old} \quad z_{old}]$ may be floating point numbers but the value at that point can be interpolated from the vertices of the $2 \times 2 \times 2$ cube the point falls in. This method is used at least once solely on the labelmaps in the process to extract the plots of cross sectional areas along the length. Since the new interpolated voxels fall on a single plane they can be treated as "pixels". The number of such

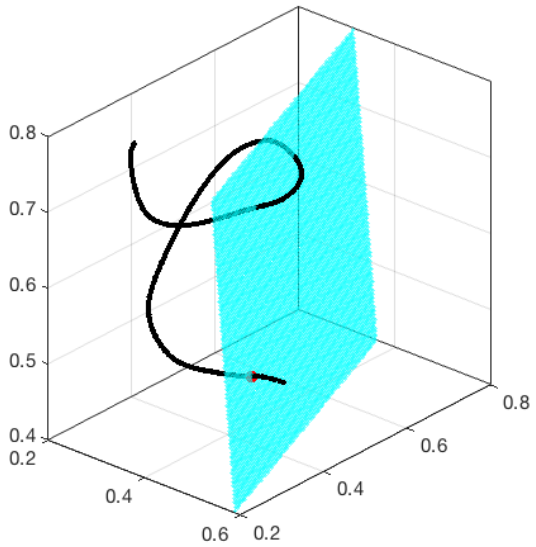

Figure 15: New interpolated plane at a point along the reparameterized medial axis. The red dot shows the point at which the medial axis is normal to the plane.

pixels in the interpolated plane in the labelmap, can be multiplied by the pixel area (16μm × 16μm) to get the cross sectional area of the scala at that point along the medial axis. To extract concentrations, the new interpolated labelmap and μCT planes are superimposed on each other and voxel values are averaged only over regions where they intersect. To ensure that the extraction does not include bone, the planar labelmap is eroded at least once before averaging is performed.

4.6.2 Volumetric Extraction

The process is fairly simple and involves using a predefined spherical mask at each point along the medial axis. The final mask at each point is the intersection of the sphere and the whole 3D labelmap, to ensure we do not surpass the borders. With this method, we do not need the earlier step for reparameterization and the raw medial axis can be made use of. This method may be used preliminarily as a qualitative gauge that tells us if the experiment was successful, but since it not only averages across the scala but also across its length causing an unintended smoothing of the extracted HU and resulting concentration values.

For the concentration extractions, we use the planar method in the baseline and 5 subsequent scans with a disc that is 7 voxels in diameter. The difference between those values and those of the baseline, result in the final extracted concentration profile for each scan. In larger scalae, the difference in both the

methods of extraction is usually small with the volumetric extraction being slightly smoother. However, in smaller regions like spiral ligament, both methods may prove to be problematic since in either case it is has very few voxels for averaging.

4.6.3 Baseline correction

Voxels within each scan represent not only the concentration of the contrast agent delivered to it, but also the underlying structures. So the "concentration" values extracted from each scan need to be corrected so that they represent only the concentrations of Iopmaidol. The intensity profiles extracted from all the 6 scans (including the baseline) using a 7 voxel planar disc are calibrated to give the corresponding concentration values. The resulting profile from the baseline scan is subtracted from the profiles extracted from the remaining scans. This is called baseline correction and also helps to mitigate some of the effects of noise. The resulting corrected concentration profiles are used in the inverse model and optimizer for parameter extraction.

5 Parameter Extraction

Though the model can be treated as a set of linear equations in terms of the transfer coefficients, a simple linear inversion of matrices cannot be used since the time interval for each scan is 20 minutes with another interval of 10 minutes between each scan. The equations themselves are partial differential equations in x and t. To discretize them, Δt needs to be less than 1 second, or the equations break down. Instead we apply a stochastic gradient descent approach while trying to minimize the sums of normalized mean squared errors of each scala.

$$\mathscr{L} = \frac{MSE(C_{ST})}{\mu_{ST}^2} + \frac{MSE(C_{SM})}{\mu_{SM}^2} + \frac{MSE(C_{SV})}{\mu_{SV}^2} \tag{44}$$

The loss is treated as a function of the parameters and they are then incremented at a rate proportional to the derivative of the loss with respect to that parameter. We discuss the process further in this section.

5.1 Forward model: Discretization of Equations

Consider the concentration $\bar{c}(x,t)$ within a scala along the length x, with cross sectional area S(x) and volume V(x) where $V(x) = S(x)dx$

$$\frac{\partial \bar{c}(x,t)}{\partial t} = \frac{1}{S(x)}\frac{\partial}{\partial x}\Big(D(x,t)S(x)\frac{\partial \bar{c}(x,t)}{\partial x}\Big) - \frac{KA(x)}{V(x)}(\bar{c}(x,t) - \bar{b}(x,t)), \tag{45}$$

$$x_0 \leq x < L$$

$$\frac{\partial \bar{c}(L,t)}{\partial x} = 0, x = L$$

$$\bar{c}(x,0) = \bar{c_0}(x), t = 0$$

where K denotes the transport coefficient across the membranes between scalae and $b(x,t)$ is the concentration in a neighbouring scala. The diffusion coefficient is concentration dependent as in Eqn 9. But since the concentration is itself a function of x and t, the diffusion coefficient can also be considered a function of x an t.

Using Product rule

$$\frac{\partial \bar{c}(x,t)}{\partial t} = D(x,t)\frac{\partial^2 \bar{c}(x,t)}{\partial x^2} + \frac{1}{S(x)}\frac{\partial \bar{c}(x,t)}{\partial x}\frac{\partial}{\partial x}\Big(D(x,t)S(x)\Big) - \frac{KA(x)}{V(x)}(\bar{c}(x,t) - \bar{b}(x,t)) \tag{46}$$

Using product rule and discretizing the equation so that the length of the scala is divided into infinitesimal parts of length Δx and the difference in time steps is Δt we get

$$\frac{\Delta \bar{c}(n,i)}{\Delta t} = D(n,i)\frac{\Delta^2 \bar{c}(n,i)}{\Delta x^2} + \frac{1}{S(n)}\frac{\Delta \bar{c}(n,i)}{\Delta x}\Big(\frac{\Delta D(n,i)}{\Delta x}S(n) + \frac{\Delta S(n)}{\Delta x}D(n,i)\Big) - \frac{KA(n)}{V(n)}(\bar{c}(n,i) - \bar{b}(n,i)) \tag{47}$$

For the purpose of the model, at every new instance in time, we can consider

$$\bar{c}(x,t) = \bar{c}(x,t_{-1}) + \Delta t\frac{\partial \bar{c}(x,t)}{\partial t} \tag{48}$$

Since each scan is taken over a 20 min period, we can simulate a similar case by averaging the above equation over the total number of discrete time steps K it takes to reach 20 minutes, $I = 60 \times 20/\Delta t$

$$C(n) = \frac{1}{I}\sum_{i=1}^{I}\Big(\bar{c}(n,i-1) + \Delta t\frac{\Delta \bar{c}(n,i)}{\Delta t}\Big) \tag{49}$$

$$C(n) = \frac{1}{I}\sum_{i=1}^{I}\Big(\bar{c}(n,i-1) + \Delta \bar{c}(n,i)\Big) \tag{50}$$

C(n) is the estimated concentration averaged over 20 minutes at n, so that it can be compared to the corresponding concentration extracted from the scans and I is the number of discrete time steps it takes to reach 20 min.

5.2 Parameter Optimization

We assume that the loss is a function of the parameters we try to optimize. Starting with an initial estimate of the transfer coefficients and D_0, we run the forward model. We normalize the resulting simulated concentration profiles as well as the extracted concentrations profiles with respect to the maximum concentration observed in the scala tympani within our scans. We compare the normalized simulated concentrations to the normalized extracted ones and calculate the loss, which is in a multidimensional space. We look for the best possible minima in this multidimensional space by incrementally changing the parameters at a rate proportional to the derivative of the loss (with respect to that parameter). This is

done using a hyper-parameter called the learning rate usually denoted by α. It is used to scale the derivatives and acts as a deciding factor in how fast the optimization converges.If C_{scan} denotes the original extracted concentrations and C_max denotes the maximum concentration extracted from a voxel within the registered scala tympani, the Loss for a single 20 min scan would be

$$\mathscr{L} = \frac{1}{N}\sum_{n=1}^{N}\Big(\frac{C(n) - C_{scan}(n)}{C_{max}}\Big)^2 \tag{51}$$

To make updates in the parameters, we require the first derivatives of the loss with respect to the respective parameter. But since we use a discretized set of differential equations, calculating the derivatives analytically would be a non trivial problem. Instead, we make an incremental change in the parameter for the first iteration and then increment it based on the rate of change of the loss with respect to the parameter itself which is calculated by assuming finite differences.

$$\frac{d\mathscr{L}}{dK} = \frac{\mathscr{L} - \mathscr{L}_{-1}}{\Delta K} \tag{52}$$

$$\frac{d\mathscr{L}}{dD_0} = \frac{\mathscr{L} - \mathscr{L}_{-1}}{\Delta D_0} \tag{53}$$

$$\frac{d\mathscr{L}}{d\gamma} = \frac{\mathscr{L} - \mathscr{L}_{-1}}{\Delta \gamma} \tag{54}$$

$\mathscr{L}$ represents the loss from the current iteration and $\mathscr{L}_{-1}$ represents the loss calculated from the previous iteration.

The parameter update process is detailed in the steps below.

---

(1) Randomly initialize parameters K, γ and D_0

(2) Initialize hyperparameters $\alpha_K, \alpha_{D_0}, \alpha_\gamma$ to low values

(3) Run the forward model with the ranodmly intialized parameters

(4) Calculate the loss $\mathscr{L}$ for this simulation

(5) Make incremental changes in K, D_0 and γ

$K \leftarrow K + K \times 10^{-4}$

$D_0 \leftarrow D_0 + D_0 \times 10^{-4}$

$\gamma \leftarrow \gamma + \gamma \times 10^{-4}$

(6) Use the new parameter values in the forward model again

(7) Calculate the loss $\mathscr{L}$ for this iteration

(8) If the change in loss is less than 0.01%

Save parameters and exit loop

Else update parameters again

$K \leftarrow K - \alpha_K \frac{d\mathscr{L}}{dK}$

$D_0 \leftarrow D_0 - \alpha_{D_0} \frac{d\mathscr{L}}{dD_0}$

$\gamma \leftarrow \gamma - \alpha_\gamma \frac{d\mathscr{L}}{d\gamma}$

Repeat from step (5)

If the initial parameter estimates selected are close to the values of a minima, the gradient descent method will be to find those values if the values of the learning rates are small enough. If the learning rates are too large we may overshoot the global minima and end up in another local minima. The same process may be carried out to estimate the flow rate at each time point while taking into consideration just the point of delivery with the initial assumption that the flow rate is equal to 32nL/min (the flow rate for the experiment).

It must be noted that this method requires some brute force and may need to be run a few times with varied initial values of hyperparameters and parameters before reaching an optimal solution.

6 Results and Discussions

The parameter optimization was run on multiple datasets with each containing five 3D μCT scans (and an extra baseline scan) taken over 140min, while 490mg/ml of Iopamidol (240mg/ml of organically bound Iodine) was being infused at 32nl/min. Each scan took about 20 min with a set up time of 10 min between scans. The optimization was run with randomly initialized parameters until the change in the loss was negligible (0.01% of the loss in the previous iteration). The final parameters selected were those associated with the lowest loss. As is the case with gradient descent the selection of initial parameters (which is random) determines whether the algorithm converges and if it does, how soon it happens. So the convergence occurred within the first 10 iterations if the initial estimates of the parameters were close to the values at the minima.

After convergence, each parameter was averaged over its respective extracted values from the experiments. These values were used for all simulations thereafter. These parameters were adjusted to be applied to other drugs as will be discussed later in the chapter.

6.1 Extracted concentration profiles

Using the planar extraction as discussed earlier, the HU values within a disc of 7 voxel diameter are averaged at every point along the medial axis of each scala. Based on the calibration curve, the HU values give us the concentration profiles along the length of each scala after baseline correction. The extracted concentrations at 5 time points for two of our experiments normalized to the delivered concentrations are given in the figure 16.

It can be seen that the profiles within ST show a decreasing trend in the concentration as we go along the length, until we reach 40-50% where it almost starts to plateau. This can be attributed to the concentration dependent diffusion coefficient. The maximum concentration in ST represents the point of delivery. In the first experiment, the maximum keeps increasing for each curve, instead of being close to 1. This suggests the presence of a leak, which lead us to estimating the flow rate at that point. The dip in the profiles of the first time point at 10 min in ST are due to the presence of an air bubble which gets absorbed over time. We also note that, the concentrations within SM track those within ST. We now provide the parameters learned and the simulated concentration profiles.

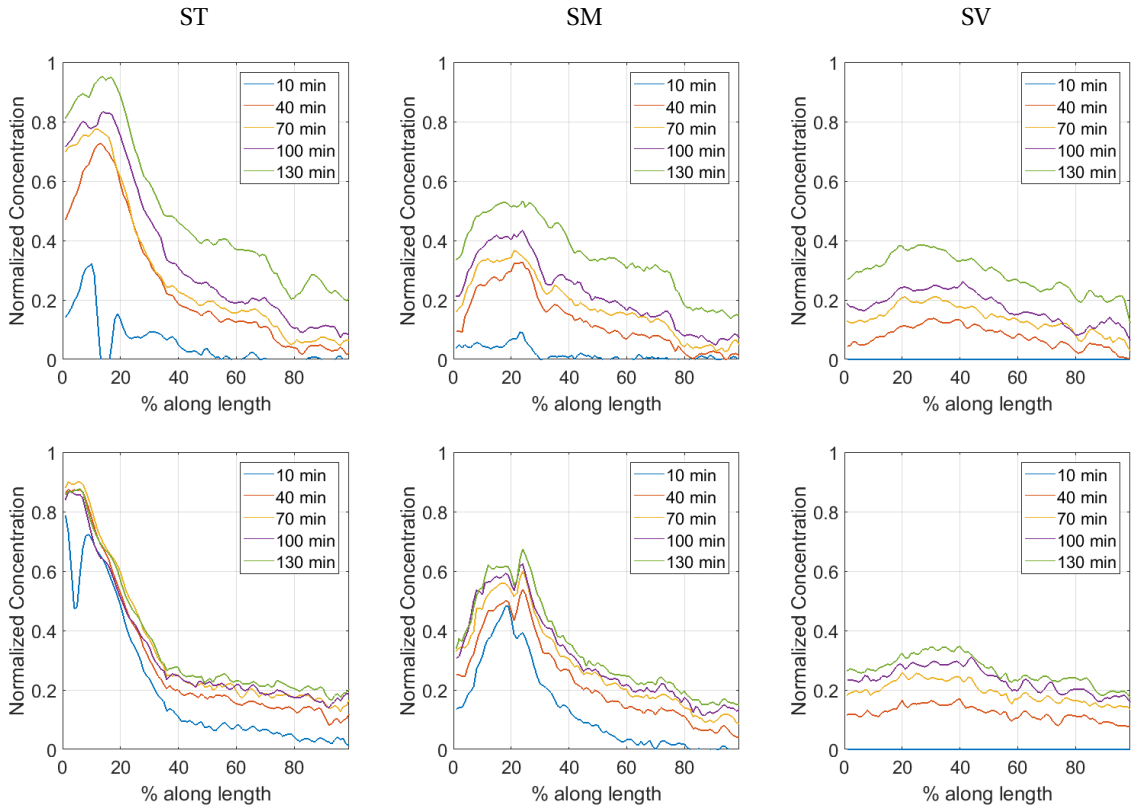

Figure 16: Normalized extracted concentrations from the 5 consecutive scans from 2 experiments, are plotted against the length of each scala in percentage. Each curve is labeled by the mean time point of the 20 minutes over which the corresponding scan was taken. The maximum value of each curve within ST indicate the point of delivery. The concentrations in ST for the April 9th scans (first row) show a steady increase in the maximum value over time while in the June 21st scans, they remain fairly constant. This could be explained by a leak that gets filled up over time. The dips in the 10min curves are due to the presence of an air bubble that dissipates over time.

6.2 Learned Parameters

For each experiment, we learned the three transfer coefficients, K_{ST-SM}, K_{SM-SV} and $K_{SM-clear}$ (where K_{i-j} denotes the transfer between scalae i and j), the average flow rate per scan, and the parameters for the adaptive concentration dependent diffusion coefficient. The relation used for the concentration(in v/v, c_v) dependence of the coefficient was

$$D(c) = \frac{D_0}{(1-\gamma c_v)^2} \tag{55}$$

D_0 is the limit of the diffusion coefficient when the concentration tends to 0, and γ determines the concentration at which the diffusion coefficient starts to change. D_0 can be theoretically calculated from the relation mentioned earlier

$$D = \frac{k_B T}{6\pi\eta r_H} \tag{56}$$

$$r_H = \left(\frac{3MW}{4\pi\rho\mathcal{N}_0}\right)^{1/3} \tag{57}$$

where, k_B is Boltzmann's constant, $\mathcal{N}_0$ is Avogadro's number, T is the temperature in Kelvin (311K), MW is the molecular weight of the solute (777.08g/mol) and ρ is the density of the pure solute (2.204kg/L). The viscosity η refers to the viscosity of the solution it is diffusing into, which would be perilymph in this case. Since the viscosity of perilymph in the mouse ear is unknown, we substituted it with the available value for the viscosity of water at 37°C which is 0.68cP. This gave us a value of $D_0 = 6.7 \times 10^{-4} mm^2/s$. Since this would not be the precise value for the mouse, with our optimization we would learn both, D_0 and γ. It was observed that the value of D_0 extracted from the model was $6.22 \times 10^{-4} mm^2/s$ (which is close to the value we calculated).

In his PhD thesis, Luca Fontanive [23] empirically finds the values of the diffusion coefficient of various iodinated contrast agents as they diffuse into a solution of Trisodium Phosphate in water at 6 different concentrations using diffusional ordered spectroscopy. It can be seen in Fig 17 that the points from his data fall within a similar range of values as our curves and also has a similar trend. However, the points do seem to fall off much faster than our curves as we increase the concentration. This difference is probably since we assume diffusion through perilymph while he assumes it through a solution of TSP in water. He suggests that at higher concentrations, Iopamidol tends to group together with TSP leading to the formation of "aggregate" molecules with higher molecular weight and thus higher hydrodynamic radius causing the diffusion coefficient to fall off rapidly.

The first 3 rows in table 1, show all the parameters we extracted for each experiment. The last row compares them with the values used by Plontke et al. in their work [14]. It should be taken into account that Plontke's experiment was carried out for a guinea pig ear with methylprednisolone instead of Iopamidol. Along with Salt et al. [7, 24], they suggest that the spiral ligament plays an important role in substance transport between scalae, with substance entering SM and SV through the ligament. However, these observations can be true for the guinea pig since the area of contact between ST and the the ligament is quite large.However, in the case of the murine cochlea, the area of contact between the spiral ligament and ST is negligible suggesting it may not be a major route of transport. These observations together could account

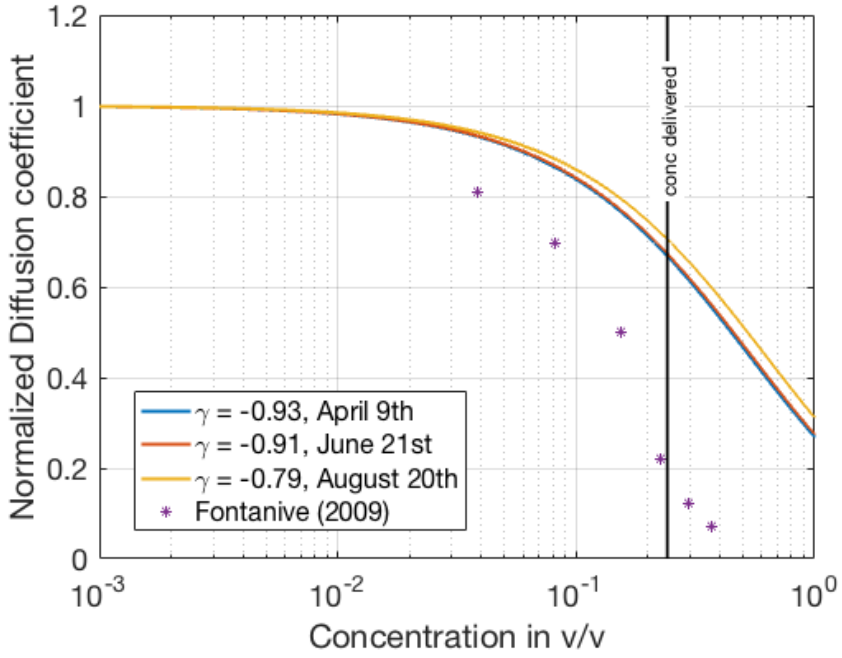

Figure 17: The y axis has been normalized by the extracted diffusion coefficient at 0 concentration for Iopamidol ($D_0 = 6.22 \times 10^{-4} mm^2/s$. The points are based on the diffusion coefficients of Iopamidol in a solution of Trisodium phosphate in water, studied in Luca Fontanive's thesis[23] and the remaining curves represent the extracted γ parameter for each experiment. In the curves, the normalized coefficient plateaus off towards 1 as the concentration tends towards zero. As the concentration begins to tend towards 1, a state where the solution mostly consists of Iopamidol, the diffusion coefficient tends to a much lower value which represents self-diffusion. While Fontanive's points are close to our curves and follow a similar trend, as we go towards a concentration of 1, their diffusion coefficient reduces much faster. Fontanive suggests that this happens at higher concentrations in their experiments since TSP forms a larger number of aggregate molecules with Iopamidol effectively increasing the size and radius of the particles in the solution. The black line shows the maximum value of concentration delivered in our experiments, so all the values of the diffusion coefficients used by the model will lie to the left of this line.

for the fact that their value for K_{ST-SM} is lower than K_{SM-SV}.

Initially we assume that the flow rate in scala tympani is 32nL/min, but our experiments have shown that instead of the concentrations being constant at the point of delivery, they increase sharply over time for some experiments. It can be seen in the first time point of 10min in the extracted concentration profiles in 18(a), that the concentration at the peak (point of delivery) is much lower but levels off in the later time points, which suggests the presence of a leak. So along with the diffusion and transfer parameters, we decided to learn the flow rate. Since each scan gives us a time resolution of 20 min, we found the average flow rate for each 20min scan and interpolated the flow rates between them. This allowed us to match

Diffusion Coefficient	Exp	K_{ST-SM} $(\times 10^{-3} mm/s)$	K_{SM-SV} $(\times 10^{-3} mm/s)$	$K_{SM-clear}$ $(\times 10^{-3} mm/s)$	D_0 $(\times 10^{-4} mm/s)$	γ
Adaptive curve	April 9th	0.71	0.35	0.042	6.23	-0.93
	June 21st	1.2	0.29	0.032	6.22	-0.91
	Aug 20th	1.1	0.52	0.033	6.23	-0.79
	Mean values	1.01	0.38	0.035	6.226	-0.87
Plontke's Experiment*		0.4	0.6	0.018**		

Table 1: Parameters extracted using our adaptive diffusion coefficient curve.
* The last row shows values used by Plontke et al. in their experiment for methylprednisolone.
** They assume clearance out of spiral ligament so the value in the last cell in the last row refers to $K_{SL,clear}$

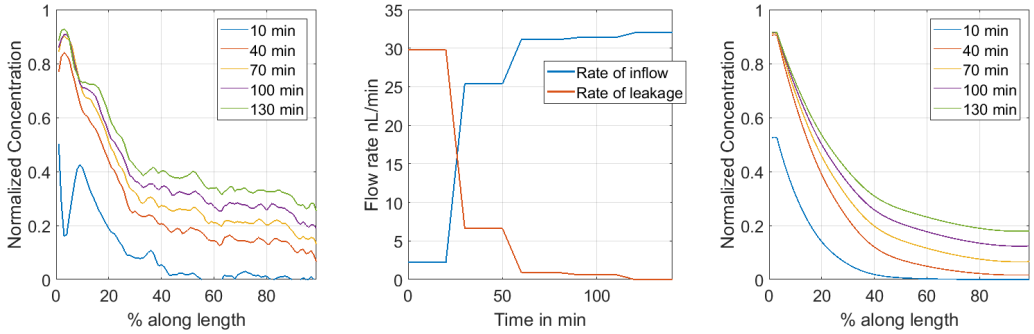

(a) (b) (c)

Figure 18: The extracted profiles on the left show the lower concentration at the first time point. The simulated profile (right) was adjusted after learning the inflow rate (center).We learned the average inflow rate each scan in the extracted profile by assuming the same flow rate over every 20 min cycle and interpolating between them. The rate of leakage is essentially the inflow rate subtracted from the flow rate administered by the pump.

our simulations to the extractions much better. This can then be subtracted from the initial estimate of 32nL/min to give us the rate of leakage of the substance. We suggest the leak takes place out of the cochleostomy site, before stabilizing.

6.3 Loss Sensitivity Analysis

As mentioned earlier, in gradient descent the parameters are updated based on the rate of change of the loss function with respect to the parameter. So it could be useful to see how sensitive the loss function is to

the optimized parameters. To do this we compute the second order derivative of the loss function at those set of parameters in a process similar to Section 5.2. This tells us the degree of curvature of the function in the direction of that parameter. A large positive value indicates that the curvature is sharply concave and a small change in the value of this parameter would result in considerable changes in the loss. Conversely a small positive value indicates that the minima is fairly flat in the direction of that parameter and even large changes in it may not affect the loss.

Exp	$\frac{\partial^2 \mathscr{L}}{\partial K^2_{ST-SM}}$	$\frac{\partial^2 \mathscr{L}}{\partial K^2_{SM-SV}}$	$\frac{\partial^2 \mathscr{L}}{\partial K^2_{SM-clear}}$	$\frac{\partial^2 \mathscr{L}}{\partial \gamma^2}$
April 9th	7.83×10^{-4}	1.5×10^{-3}	1.36×10^{-2}	3.20×10^{-7}
June 21st	7.3×10^{-4}	2.4×10^{-3}	1.92×10^{-2}	6.99×10^{-8}
Aug 20th	10×10^{-4}	1.5×10^{-3}	1.72×10^{-2}	5.62×10^{-7}

Table 2: The table shows the values of the second order derivative of the loss with respect to the parameter. It is evaluated at the minima that our optimization has reached.

Table 2 shows the values of the second order derivative of the loss for each experiment with respect to the extracted parameters evaluated at the local minima i.e. evaluated at the corresponding values extracted in Table 1. We see that the second order derivative is much lower for γ than for the transfer coefficients, indicating that its value is quite flexible in comparison to the other parameters. This is supported by the fact that during our simulations, we mostly stay in the flat part of the diffusion curve where small changes in γ may not affect our accuracy by much. Though to a lesser extent this can also be observed for K_{ST-SM}, while K_{SM-SV} and $K_{SM-clear}$ have much higher values indicating that they are much more sensitive than the other parameters.

6.4 Simulating Extracted concentration profiles

The parameters learned above change over iterations as they go through the optimization multiple times. Once the change in loss is negligible, the average of each of those parameters across experiments is used for any forward simulations henceforth. Here we show the simulated concentration profiles associated with the averaged parameters shown in Table 1 for the 21st June scans.

Fig 19 compares the extracted concentration profiles to the simulated ones while providing the error

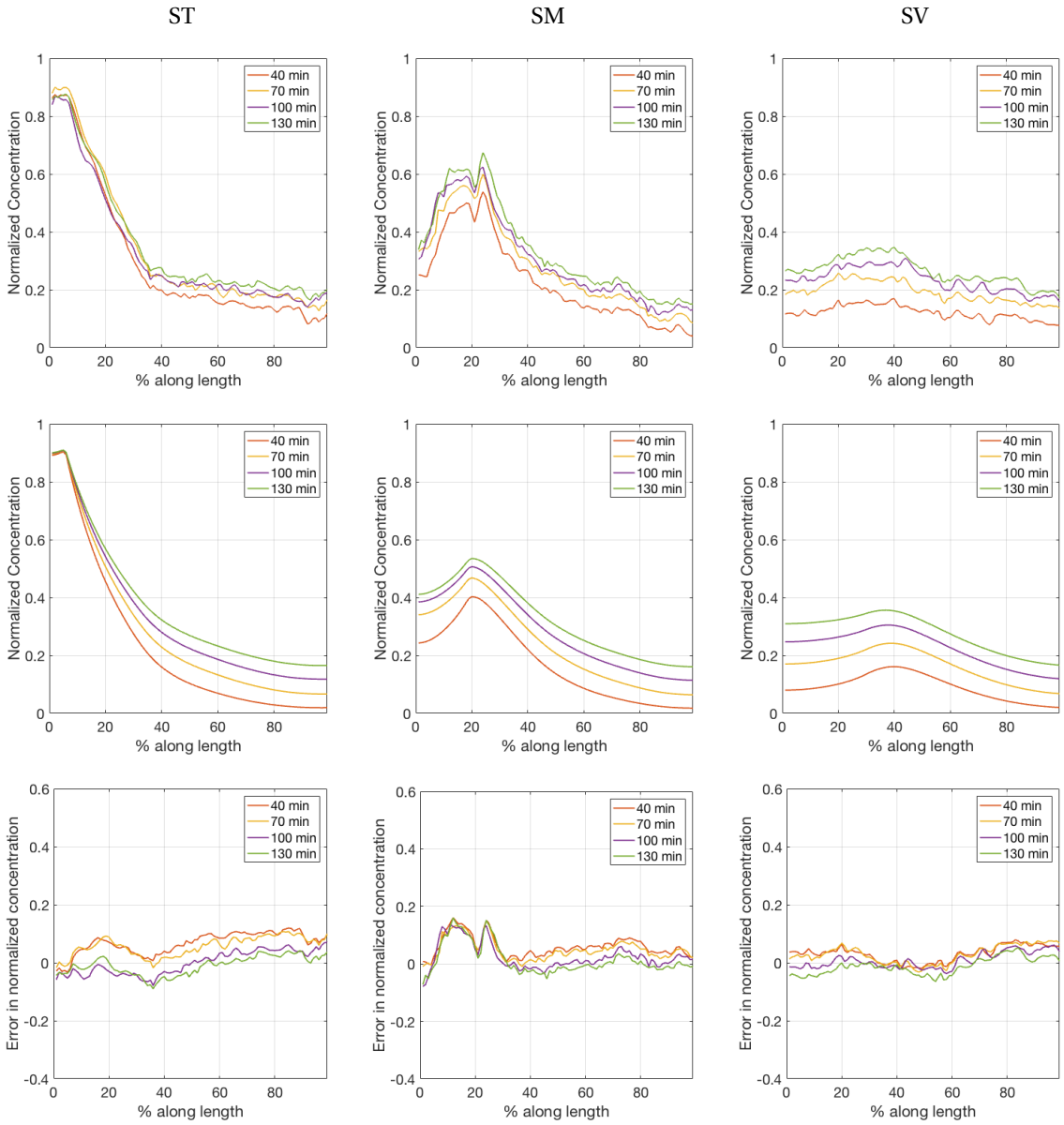

Figure 19: The plots in each column are for ST, SM and SV respectively. Each row subsequently shows the extracted concentration, the simulated concentrations using the mean of the parameters and the corresponding errors. The y-axes of all the plots represent normalized concentrations (the last row represents errors in terms of normalized concentrations) and the x-axes represent % along length.

plots. Ignoring the plots at the first time point which have a large dip the extracted concentrations due to the presence of the air bubble, the simulated plots match the extracted plots well. The RMSE for the concentration profiles is 8.9%.

Alec N. Salt came up with a model, FluidSim[13] , that takes into consideration other parts of the

cochlea such as the spiral ligament, the organ of corti, the spiral ganglion, etc, but it only considers a single fixed diffusion coefficient. The model also makes used of fixed half-times ($t_{1/2}$) to represent inter-scala communications for each membrane. Making use of the equations used in the model, which are based on his previous works [7, 24], a relation between the transfer coefficients (K) and the half-times can be calculated at each point along the length. If we consider a small cross section of volume V out of which the solute is diffusing, with area of contact A, then the half time and transfer coefficient would be related by

$$\frac{0.693}{t_{1/2}} = \frac{KA}{V} \tag{58}$$

The term $\frac{0.693}{t_{1/2}}$ is known as the rate constant. This term is multiplied by Δc across the membrane to get the change in concentration over time. We see that the relation would provide a rate constant that varies across the length of the scala. Salt handles this by allowing for the half times to be normalized by area. It must also be noted that the same half-time cannot be used to represent transport across the membrane in both directions. For example, the half time for transport to take place from SM-SV is not the same as that from SV-SM, and must be scaled by the ratio of the cross sectional areas (or volumes) of SM to SV. Salt manages this by asking the user to specify half-times only in certain directions, like one can set the half-times from organ of corti to ST but not vice versa. This is not an issue faced by our model due to the use of a transfer coefficient which remains independent of direction.

We compare our results to Salt's in FluidSim v3.14 by attempting to replicate an ideal case of our experiments where we would have no leak. With the perfusion option at 32nL/min for 490mg/ml, FluidSim was run for a solute of molecular weight 777.08g/mol with the total delivery time of 140 min. To estimate half-times that could be used in FluidSim, we used Eqn 58. For interscala half-times we estimated their values at the first point along the length. This allowed for them to be scaled in FluidSim, based on the cross sectional area as we go down the length (using the option for "scaling based on area"). The half-time for SM-SV was 6.2min (V = $5.7 \times 10^{-3} mm^3$, A = $27.2 \times 10^{-3} mm^2$), SM-OC was 6.8min (V = $5.7 \times 10^{-3} mm^3$, A = $9.9 \times 10^{-3} mm^2$), with OC-ST set to a minimal amount (0.1 min indicating nearly immediate transport between the organ of corti and ST). This was done since FluidSim did not have the provision to represent transport between ST and SM directly. Since FluidSim allows the use of a mean half-time for clearance the mean values of the area of contact and the volume of the scala were used to get a half time of 70min (V = $4 \times 10^{-3} mm^3$, A = $17.7 \times 10^{-3} mm^2$). The results generated by FluidSim and by our model shows curves that fall in similar ranges of values, but the plots generated by by our model fall with a sharper gradient. The

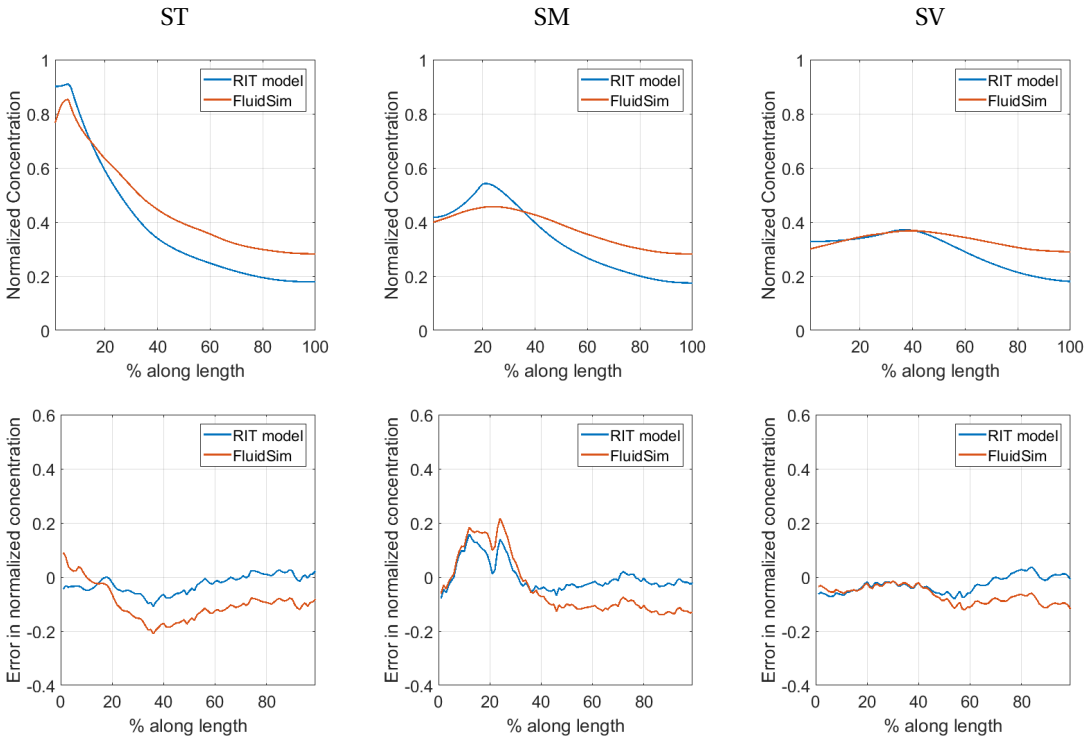

Figure 20: The plots show the concentrations in ST, SM and SV at 140 min, simulating Iopamidol delivery using our model (in blue), and those generated using Salt's FluidSim software (in red). We used the average values of the extracted transport parameters in our model. The half times for FluidSim were calculated from our transfer coefficients based on Eqn 58. The half-times used for interscala transport were 0.1 min for transport from organ of corti (OC) to ST, 6.2 min from SM to OC, 6.8 min from SM to SV while setting the option for scaling by area. For clearance out of SM, the average half-time set was 70 min. While the 0% in ST for FluidSim is assumed to be the tip of the hooked region near the round window, the curves displayed here have been adjusted so that the cochlear aqueduct is aligned for both the models. The resulting concentrations have been compared to our most consistent experiment with no leakage that was conducted on June 21st. It can be seen that our simulations are able to provide better estimates with lower errors, while FluidSim simulations result in higher errors.

curves simulated by FluidSim show a slower gradient with higher apical values in all the scalae with SM and SV showing lower basal values but uniform plots throughout. While we do include a concentration dependent diffusion coefficient in our model, its range of values ($4.5 \times 10^{-4} mm^2/s$ to $6.22 \times 10^{-4} mm^2/s$) is small and comparable to the constant coefficient used in FluidSim ($5.9 \times 10^{-4} mm^2/s$). It must be noted from the equations used in our model that we scale our transfer coefficients and clearance by multiplying them by the area of contact of the membrane in consideration and dividing the volume of the cross section out of which we are diffusing (as in Eqn 24). However FluidSim does not take into account the area of contact and scales the interscala communication half-times only by the cross sectional areas. There is

no provision to do so for the clearance and an average half time is used. This probably explains why FluidSim overestimated the concentrations in this experiment. The inclusion of the area of the membrane and volume of the cross section to describe interscala communication in our model results in an increase in transport out of scala tympani at as we travel from the base to the apex, since the basilar membrane is wider at the base than at the apex. These terms are also used in our model to represent clearance out of scala media as well. When compard to FluidSim which uses only a single average clearance half time, it results in FluidSim underestimating clearance since the volume scala media reduces gradually from base to apex. Thus the higher rate of interscala transport and clearance out of scala media can be attributed to the way our transport parameters are scaled based on the dimensions of the scalae and the membranes in consideration.

We also find the errors between the simulations and the extracted concentrations from the June 21st scans as seen in Fig 20. The profiles from this experiment show the most consistent flow rate over the 5 scans. The simulations have a constant flow rate of 32nL/min over the whole range of time. Also in the extractions, each plot represents 20min while in FluidSim we can only show a single time point at 140min. However this should not affect the comparison too much since after such long periods of time the profiles would be nearing equilibrium. The RMSE (at 140min) for our plots is lower at 8% while it is 18% for FluidSim.

6.5 Maintaining a Target Therapeutic window

As mentioned before, the therapeutic window is an important concept in pharmacokinetics which essentially is the range of concentration of the drug over which it can act as an effective treatment. Below this range the drug is ineffective and above it, it may prove to be toxic. Instead of injecting continuously or administering a single bolus injection, it may be more suitable to deliver the drug in pulses, so that it is allowed to diffuse out towards the apex before new drug can be delivered at the base again, allowing us to stay within the therapeutic window. Our model can be made use of to adjust the delivery method so that drug is used efficiently while staying within a hypothetical therapeutic window. We adjusted our flow rate so that it was pulsatile, allowing concentration to even out across the scala before pumping drug back into the base. We used the averaged parameters from Table 1 for our diffusion and transfer coefficients, by minimizing the difference in basal-apical concentration, while maximizing apical concentration.

Let us consider C_{LT} and C_{UT} to be the lower and upper thresholds allowed by a notional therapeutic window and the basal-apical difference ΔC. First, using our mean extracted parameters, we deliver a pul-

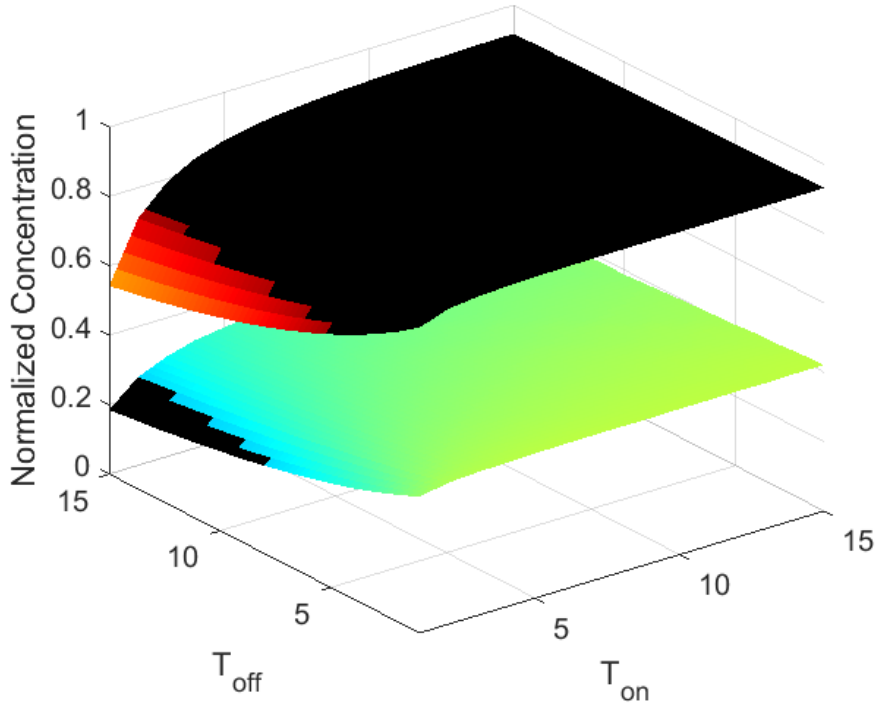

Figure 21: The figure shows maximum concentrations at the base (red and green surface) and the minimum concentrations at the apex (blue surface) recorded at equilibrium for each combination of on and off times. The black portions of each surface represent those concentrations that do not fall within the notional therapeutic window. A suitable combination for T_{on} and T_{off} would require the corresponding points in both curves to be colored and for the difference between them to be low. One such combination is for an on time of 1 min and an off time of 7 min.

sating profile near the cochlear aqueduct in our simulated cochlea. The on and off times of the pulsatile profile are varied by 1 min increments. The minimum and maximum concentrations within ST at equilibrium are saved for each combination. For this example, these min and max values are essentially the basal and apical concentrations at the end of the on cycle and at the end of the off cycle respectively, since solute reaches the base directly, and takes time to reach the apex.

We assume the delivered concentration to be 490mg/ml at 8nL/min for 2000min. The time interval is enough to reach equilibrium. If we were to assume a hypothetical case where $C_{LT} = 0.25$ of the concentration in the delivery tube and $C_{UT} = 0.75$, we could find those combinations of T_{on} and T_{off} where ΔC is minimum. In Fig. 21, we plot the maximum base values and the minimum apex values where C<0.75 and C>0.25 respectively (shown by the colored regions in the surface plots). The valid set of T_{on} and T_{off} that would stay within these thresholds, is the intersection where both the plots stay in color. Of these,

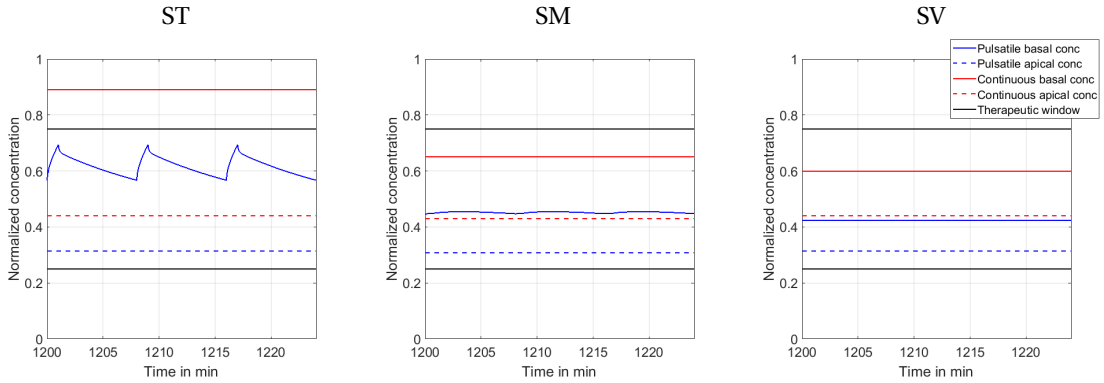

Figure 22: The figure shows concentrations in the scala tympani after equilibrium has been reached for 490mg/ml of Iopamidol (777.08g/mol) being delivered at 8nL/min continuously, as well as using a square pulse delivery which is on for 1min at 8nL/min and off for 7min. The solid black lines represent the notional therapeutic window. All concentrations must fall within these two lines so as to be effective as a drug and non-toxic at the same time. The solid and dashed colored lines show the basal and apical concentrations respectively. Red lines represent the concentration profiles over time due to continuous flow while blue shows those due to a suitable pulsatile profile. It can be seen that the pulsatile profile provides a more suitable delivery method with the basal (max) and apical (min) concentrations falling within the notional therapeutic window. But the profile at the base of ST for the continuous delivery, falls outside the window, which would lead to strong side effects.

$T_{on} = 1min$ and $T_{off} = 7min$ have the lowest difference with the maximum basal concentration at 0.38. Fig 22 shows the comparison between the resulting concentrations due to pulsatile profile after equilibrium which occurs by 1200 min since the on and off times are lower. In the basal and apical concentrations due to the pulsatile profiles with the flow rate at 8nL/min, stay within the notional therapeutic window while the continuous profile leads to excess drug delivered at the base which could lead to side-effects, while not providing much of an added advantage within the apex. By using a pulsatile profile with an on time for 1 min and off time for 7 min, it is possible to reduce the total drug delivered by 87.5% while reducing potential toxicity when compared to a continuous delivery profile, allowing a reduction in reservoir size.

The above example can be extended so that we maximize the apical concentration while minimizing the basal apical difference and maintaining the therapeutic window for all scalae. It may also be possible to come up with more complex but optimal non periodic delivery profiles. These problems would require more sophisticated optimization techniques and is left to future work.

6.6 Extension to other compounds

To compare our model to FluidSim, we simulate an experiment for the mouse cochlea in our model by scaling the averaged Iopamidol parameters extracted earlier and compare it to similar simulations from FluidSim where default values of half times for transport are used. The setup assumes 10mM (equivalent to 3.74mg/ml) of methylprednisolone is infused through a cochleostomy near the RWM at 10nL/min. In FluidSim, it is assumed that the interscala transport and half-time values for guinea pigs can be applied to mice. So for our case of the mouse cochlea, we make use of the default half times employed in FluidSim; interscala communication from SM to SV as 60 min and clearance at 110 min, we assume transport half times from SM to OC of 60 min, from OC to ST 0.1 min. All other forms of interscala communication were left unset, which FluidSim assumes to indicate infinity, or that no transport takes across that membrane. To determine the scaling factor for the parameters for methylprednisolone to be used in our model, we make use of the density of the new compound ($\rho_{new} = 1.3 g/cc^3$) along with its molecular weight. The scaling factor can be given as

$$\sqrt[3]{\frac{MW_{old}\rho_{new}}{MW_{new}\rho_{old}}} \tag{59}$$

where MW_{old} and ρ_{old} are the molecular weight and density of Iopamidol and MW_{new} and ρ_{new} are the molecular weight and density of Methylprednisolone.

We observed that in our model the concentration dependence of the diffusion coefficient does not come into play at such low concentrations where it is close to D_0. We also observed that our effective diffusion coefficient of $6.65 \times 10^{-4} mm^2/s$ is close in value to the one used in FluidSim $7.84 \times 10^{-4} mm^2/s$. On converting the half-times used in FluidSim to corresponding transfer coefficients, by using the scaling factor in expression 59, we found that while the values for clearance were comparable, the transfer coefficent equivalents of the default half times used in FluidSim were much lower than our estimates of the transfer coefficients (which were scaled versions of the coefficients extracted for Iopamidol), indicating that interscala transport for the experiment in FluidSim was assumed to be much lower.

Looking at Fig 23, we see that for the FluidSim plots, with interscala transport being slower and the diffusion coefficient being constant in FluidSim, longitudinal movement of the solute is freely allowed to take place via diffusion while the amount of solute entering or leaving the comparment due to transverse permeation is low, this results in a flatter profile as substance moves towards the apical regions while only small amounts get added to or removed from it. While this is easily observed in SM, the concentration profile in SV is also fairly flat except for the slight increase towards the apex. This may be due to some

solute entering SV from ST via the helicotrema but the differences in the apical values of ST and SV may suggest a deficiency in the details of the model. Conversely in our model, while the diffusion coefficient can be treated as constant, transport between compartments takes place at a higher rate, so some substance can move out of or into another scala before it reaches the apex, resulting in a higher gradient in the concentration profile of ST. This also results in the maintenance of a small peak in SM which tracks the peak in ST, and maintains the gradient in SV. We noted earlier that the transfer coefficients in our model was scaled by the area of contact of the membrane and the volume of the section in consideration, while the half-times for interscala communication as used in FluidSim only take the cross sectional areas (representative of the cross sectional volume) into account. This suggests that the transport surface area to volume ratio is an important factor and may be used to scale the half times between animals. We considered the case of two small cylinders with cross sectional areas similar to those of the mouse and guinea pig, and attempted to scale the half times based on the ratio of a section of the curved surface area to the volume. The section was considered to be subtended by the same angle meaning that proportions were maintained while scaling between the mouse and guinea pig. This however suggested that the scaling of half-times is only dependent on the ratio of the radii of the 2 cylinders. The approximate radius in the basal region of ST is 0.203mm in the mouse, while it is 0.683 in the guinea pig. The ratio of the two is 3.15 which is used to scale down the half-times from the guinea pig to the mouse. We performed a simulation with these scaled half times but found that it only made a very small difference in the profiles in ST and SV but not in SM. This suggests that more investigation needs to be done on the way these parameters are scaled between animals.

	Half-times used in FluidSim (min)		$\Longrightarrow$	Equivalent transfer coefficients ($\times 10^{-3}$mm/s)		Transfer coefficients used in our model ($\times 10^{-3}$mm/s)	$\Longrightarrow$	Equivalent half-times (min)
	Default	Scaled		Default	Scaled			
SM-ST*	60	20		0.10	0.30	1.08		5.5
SM-SV	60	20		0.036	0.108	0.40		5.4
SM-clear	110	36		0.024	0.072	0.038		70
D or D_0	$7.84 \times 10^{-4} mm^2/s$					$6.65 \times 10^{-4} mm^2/s$		
γ						-0.87		

Table 3: Transport parameter estimates for Methylprednisolone are shown in this table. The first column shows default vales of half times given for a mouse in FluidSim (which are the same half times as guinea pig). The corresponding equivalent transfer coefficients are calculated using Eqn 58. When compared to the translated transfer coefficients used by our model, they are much smaller indicating very low interscala transport. The fourth column shows the corresponding half times for the transfer coefficients used by our model. They seem to be much lower than the default values set in FluidSim, thus suggesting transport that occurs more freely. This makes sense considering the size of the molecule is smaller than Iopamidol.

Using our estimates of the parameters for methylprednisolone, we also simulate an experiment similar to Section 6.5. We saved out the minimum and maximum values for each combination of on and off times of a pulsatile profile, and determined that for a notional therapeutic window of C_{LT} = 0.25 and C_{UT} = 0.75 for 10mM of methylprednisolone delivered in the base of ST, a pulsatile profile with on times of 2 min and off times of 12 min would be most suitable. It must be noted that such a window is very small (representing a range of only 1.87mg/ml) at such low concentrations. It can be maintained within such small windows since the concentration dependence of the diffusion coefficient can be ignored at such low concentrations, meaning that more solute is available to diffuse out towards the apex. Using a pulsatile profile as shown by the blue lines in Fig 24 that stay within the black lines of the notational therapeutic window could prove to be safer and more efficient. With this pulsatile profile with an on time of 2 min and off time of 12 min, 85.7% less drug can be delivered when compared to a continuous delivery, reducing required reservoir volumes and potential toxicity.

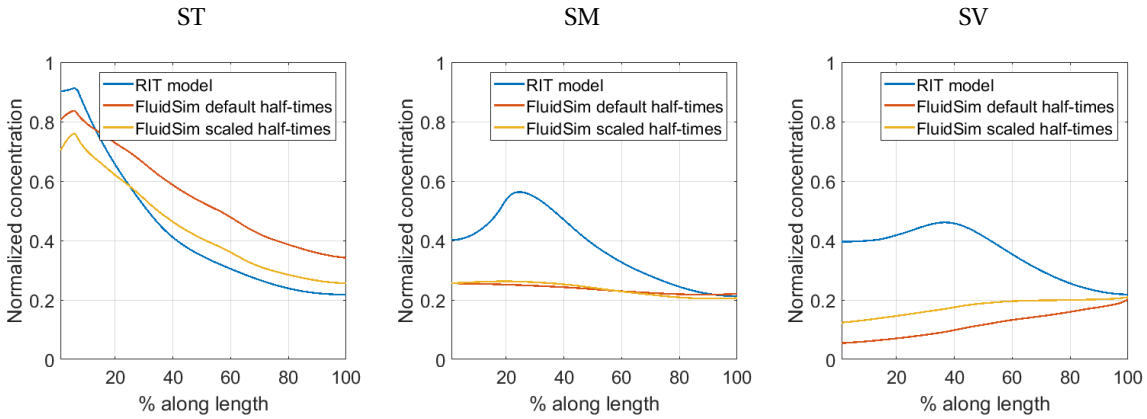

Figure 23: The plots show concentrations in ST, SM and SV of the mouse cochlea with 10mM of methylprednisolone being delivered to it at 10nL/min for 140min. The curves for the RIT model were generated using a scaled version of the average transport parameters extracted from Iopamidol experiments. Half times for interscala communication in FluidSim were assumed to be 60 min for transport from SM to SV and from SM to OC; and 0.1 min from OC to ST, with the option for scaling by area set. The average clearance half time out of SM was assumed to be 110.9 min. These half-times were the same as those used for guinea pig. We also plotted results for scaled versions of the half times. We see that the curves differ significantly in concentration values for SV and SM. Scaling the half times improves the fit for ST but has a minimal effect on SM and SV.

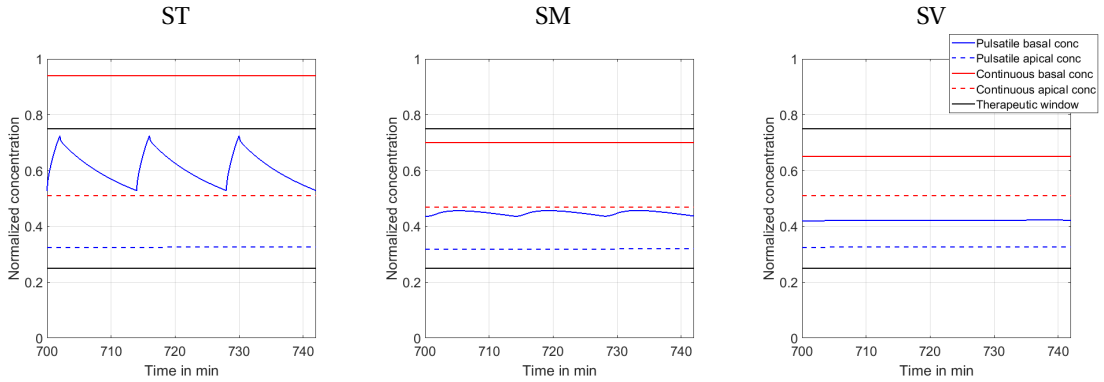

Figure 24: The figure shows delivery of methylprednisolone at 10mM or 3.74mg/ml of methylprednisolone are delivered through a cochleostomy at 10nL/min in a manner similar to section 6.5. Using a pulsatile profile at the base, with an on time of 2 min and off time of 12 min, our concentration profiles (blue lines) are able to stay within the window (black lines). Using a continuous flow (red lines) would have been detrimental in this case as the basal concentration would have exceeded the therapeutic window.

7 Conclusions

We made use of micro-computed Tomography as a non-invasive method for sampling the concentration of the contrast agent within the principal compartments of the cochlea. Using the extracted profiles we were able to extract transport parameters in our 1D model for each experiment, and simulate concentration profiles similar to the ones sampled from the scans, confirming the reasonable accuracy of our models. Using averages of the parameters extracted, and given the upper and lower concentration thresholds of a notational therapeutic window, we were also able to simulate concentration profiles that optimized a pulsatile delivery to minimize base to apex concentration gradients while maximizing apical concentrations.

The diffusion model in this work was based solely on the principal three scalae of the cochlea, scala tympani, scala vestibuli and scala media. This was primarily due to the fact that intensity values extracted from much smaller regions like the organ of corti and the spiral ligament (SL) could not be trusted because the number of voxels in these regions were very low and were not enough to overcome the presence of noise. The labelmap for SL would often overlap with regions of high intensity suggesting the presence of bone. We had difficulty in determining whether SL was well registered in the labelmaps for the μCT scans due to the low contrast and blurred contours inherently present in CT scans. An eventual possibility in overcoming these issues is to use higher resolution CT scanners like "nano-CT" scanners [25] which would further improve spatial resolution giving us more voxels to average over. A limitation of these scanners for now is that they require samples to be of the order of a millimeter. Another approach would be to look into more sophisticated methods for registration. Work is currently underway to use machine learning on multiple sets of the μST scans, so that the registrations can be more robust. This work will also tell us more about the variability in cochlear anatomy between various mice.

By making assumptions that were as close as possible and to the conditions in one our experiments for Iopamidol, we compared our forward model to FluidSim, which is considered to be the gold standard in cochlear fluid models. While the profiles for both sets of curves were close, ours showed lower values in the apices. These differences were attributed to the fact that we scaled our interscala transport parameters by the area of contact of the membrane in consideration as well as the volume of the cross section leading to increased transport towards the apex of the scalae. Our profiles seemed to match the extracted concentrations from our experiment better than FluidSim.

We illustrated the extension of our model to other drugs based on the molecular weight and density

of the solute, but our results for methylprednisolone differed from simulations in FluidSim. The concentrations in this experiment were very low so the diffusion coefficient was fairly independent of it. On translating our average parameters extracted from Iopmaidol to Methylprednisolone, the resulting values suggested that the the rate of transport between scalae should have been higher than that observed in FluidSim. The profiles generated by FluidSim were much flatter than those generated by our model, suggesting that the drug would be allowed to move freely towards apical regions within each scala while only small amounts got added to or removed from it due to interscala communication. The discrepancies could be explained by many factors. One possibility is the way half times are set in FluidSim. Most of the work related to the simulator is done on guinea pigs, but the values for the half-times for the guinea pig are assumed to be the same as those for the mouse. This may not be an accurate representation of transport in the mouse cochlea, and more investigation is required to determine how half times are scaled between animals. Another possibility is that the method we use for the extension of our model may not be suitable for all compounds. More work needs to be done to determine how this translation needs to be handled depending on the chemical and physical properties of the drug for longitudinal transport. For the purpose of interscala transport, the properties of the membranes involved also need to be studied as they can be selective based on the molecule that is being transported (for example the basilar membrane is ionically selective when it comes to Na+ and K+ ions). This may severely affect their semi-permeability.

In the results, we observe that with the current method of delivery near the base, if the drug is being injected over a long period of time, the concentration at the apex will reach equilibrium at a lower concentration than the base since there will always be drug/contrast agent delivered to the base while transport and clearance mechanisms limit total drug transport to the apex. This may make it difficult to deliver so that the substance stays within the therapeutic window. Other methods of delivery can also be looked into, where a a long perforated capillary tube, that extends from the base to the apex is inserted through the round window membrane. Delivery can take place at multiple points along the length of ST so that much higher concentrations can be reached along the entire length.

In our experiments regarding the maintenance of a notional therapeutic window we use a simple method of running the forward simulation with different combinations of on and off times for a pulsatile profile and noting down the minimum and maximum values of the concentrations achieved at equilibrium within the scala tympani. By minimizing the differences between the minimum and maximum values while staying within the notational window, we select a suitable profile for safe drug delivery. This method is fairly simple but during selection of the appropriate pulsatile profile only considers the scala

tympani. To ensure that the treatment is effective, we need to target the hair cells and other structures on the basilar membrane, for which the window will have to be maintained within scala media as well. While concentrations in scala media do track those in scala tympani and fell within our notional window, investigation of sophisticated optimization techniques to determine a suitable delivery profile, may be necessary especially when the window has a much smaller range when compared to the range of concentrations in consideration.

The work presented in this thesis explores the possibility of extending a model derived from experiments based on the non invasive sampling of one compound delivered to the murine cochlea to other drugs. It also investigates how drug delivery profiles can be adjusted to maintain therapeutic windows even after the model has been extended. These contributions show the importance of the work in future development of safe, effective and efficient drug delivery paradigms that could be used in the treatment of acute and chronic types of hearing loss.

References

[1] E. E. Pararas, D. A. Borkholder, and J. T. Borenstein, "Microsystems technologies for drug delivery to the inner ear," *Advanced drug delivery reviews*, vol. 64, no. 14, pp. 1650–1660, 2012.

[2] A. A. McCall, E. E. Swan, J. T. Borenstein, W. F. Sewell, S. G. Kujawa, and M. J. McKenna, "Drug delivery for treatment of inner ear disease: current state of knowledge," *Ear and Hearing*, vol. 31, no. 2, pp. 156–165, 2010.

[3] K. S. Alzamil and F. H. J. L. ., "Extraneous round window membranes and plugs: Possible effect on intratympanic therapy," *Annals of Otology, Rhinology and Laryngology*, vol. 109, no. 1, pp. 30–32, 2000.

[4] S. K. R. Plontke, A. W. Wood, and A. N. Salt, "Analysis of gentamicin kinetics in fluids of the inner ear with round window administration," *Otology and Neurotology*, vol. 23, no. 6, pp. 967–974, 2002.

[5] M. Marcus, K. Rainer, A. Wolfgang, and O. Elmar, "Auditory nerve fibre responses to salicylate revisited," *Hearing Research*, vol. 183, no. 1, pp. 37–43, 2003.

[6] A. N. Salt, R. Thalmann, D. C. Marcus, and B. A. Bohne, "Direct measurement of longitudinal endolymph flow rate in the guinea pig cochlea," *Hearing Research*, vol. 23, no. 2, pp. 141–151, 1986.

[7] A. N. SALT, K. OHYAMA, and R. THALMANN, "Radial communication between the perilymphatic scalae of the cochlea .2. estimation by bolus injection of tracer into the sealed cochlea," *Hearing Research*, vol. 56, no. 1-2, pp. 37–43, 1991.

[8] A. N. Salt and J. DeMott, "Longitudinal endolymph flow associated with acute volume increase in the guinea pig cochlea," *Hearing Research*, vol. 107, no. 1-2, pp. 29–40, 1997.

[9] M. Haghpanahi, M. B. Gladstone, X. Zhu, R. D. Frisina, and D. A. Borkholder, "Noninvasive technique for monitoring drug transport through the muring cochlea using micro-computed tomography," *Annals of Biomedical Engineering*, vol. 41, no. 10, pp. 2130–2142, 2013.

[10] P. A. Santi, I. Rapson, and A. Voie, "Development of the mouse cochlea database," *Hearing research*, vol. 243, no. 1-2, pp. 11–7, 2008.

[11] A. F.Ghiz, A. N.Salt, J. E.DeMott, M. M.Henson, O. W. J. Henson, and S. L. Gewalt, "Quantitative anatomy of the round window and cochlear aqueduct in guinea pigs," *Hearing Research*, vol. 162, no. 1-2, pp. 105–112, 2001.

[12] M. Thorne, A. N. Salt, J. E. DeMott, M. M. Henson, O. W. J. Henson, and S. L. Gewalt, "Cochlear fluid space dimensions for six species derived from reconstructions of three dimensional magnetic resonance images," *The Laryngoscope*, vol. 109, no. 10, pp. 1661–1668, 1999.

[13] A. N. Salt, "Simulation of methods for drug delivery to the cochlear fluids," *Advances in oto-rhino-laryngology*, vol. 59, p. 140, 2002.

[14] S. K. Plontke, N. Siedow, R. Wegener, H. P. Zenner, and A. N. Salt, "Cochlear pharmacokinetics with local inner ear drug delivery using a three-dimensional finite-element computer model," *Audiology and neuro-otology*, vol. 12, no. 1, pp. 37–48, 2006.

[15] W. A. Yost, *Fundamentals of Hearing: An Introduction.* Academic Press, 5 ed., 2013.

[16] R. K. Hobbie and B. J. Roth, *Intermediate Physics for Medicine and Biology.* Springer International Publishing, 5 ed., 2015.

[17] H. Fujita, "The exact pattern of a concentration-dependent diffusion in a semi-infinite medium, part ii," *Textile Research Journal*, vol. 22, no. 12, pp. 823–827, 1952.

[18] C. S. Patlak, "An approximation diffusion equation for a long narrow channel with varying cross-sectional area," *Bulletin of Mathematical Biology*, vol. 35, pp. 81–86, 1973.

[19] D. A. Borkholder, X. Zhu, B. T. Hyatt, A. S. Archilla, W. J. Livingston III, and R. D. Frisina, "Murine intracochlear drug delivery: Reducing concentration gradients within the cochlea," *Hearing Research*, vol. 268, no. 1-2, pp. 2–11, 2010.

[20] Z. Xu, "3d subject-atlas image registration for micro-computed tomography based characterization of drug delivery in the murine cochlea," Master's thesis, Rochester Institute of Technology, 2016.

[21] M. Kerschnitzki, P. Kollmannsberger, M. Burghammer, G. N. Duda, R. Weinkamer, W. Wagermaier, and P. Fratzi *Journal of Bone and Mineral Research*, vol. 28, no. 8, pp. 1837 – 1845, 2013.

[22] T.-C. Lee, R. L. Kashyap, and C.-N. Chu, "Building skeleton models via 3-d medial surface/axis thinning algorithms," *Graphical Models and Image Processing*, vol. 56, no. 6, pp. 462–478, 1994.

[23] L. Fontanive, *Nanoscale Interaction for higher Efficiency of Contrast Media.* PhD thesis, University of Trieste, Trieste, Italy, 2009.

[24] A. N. SALT, K. OHYAMA, and R. THALMANN, "Radial communication between the perilymphatic scalae of the cochlea .1. estimation by bolus injection of tracer into the sealed cochlea," *Hearing Research*, vol. 56, no. 1-2, pp. 29–36, 1991.

[25] M. Müller, I. de Sena Oliveira, S. Allner, S. Ferstl, P. Bidola, K. Mechlem, A. Fehringera, L. Hehn, M. Dierolf, K. Achterhold, B. Gleich, J. U. Hammel, H. Jahn, G. Mayer, , and F. Pfeiffer, "Myoanatomy of the velvet worm leg revealed by laboratory-based nanofocus x-ray source tomography," *Proceedings of the National Academy of Sciences*, vol. 114, no. 47, pp. 12378–12383.